

SURFACE COVERAGE CONTROL OF SELF ORGANIZED PLASMONIC  
NANOSTRUCTURES AT INTERFACES OF PHOTOVOLTAICS RELATED  
MATERIALS

A THESIS SUBMITTED TO  
THE GRADUATE SCHOOL OF NATURAL AND APPLIED SCIENCES  
OF  
MIDDLE EAST TECHNICAL UNIVERSITY

BY  
GİZEM BİRANT

IN PARTIAL FULFILLMENT OF THE REQUIREMENTS  
FOR  
THE DEGREE OF MASTER OF SCIENCE  
IN  
PHYSICS

JANUARY 2017



Approval of the thesis:

**SURFACE COVERAGE CONTROL OF SELF ORGANIZED PLASMONIC  
NANOSTRUCTURES AT INTERFACES OF PHOTOVOLTAICS RELATED  
MATERIALS**

submitted by **Gizem BİRANT** in partial fulfillment of the requirements for the degree of **Master of Science in Physics Department, Middle East Technical University** by,

Prof. Dr. Gülbin Dural Ünver  
Dean, Graduate School of **Natural and Applied Sciences**

\_\_\_\_\_

Prof. Dr. Sadi Turgut  
Vice Head of Department, **Physics Dept., METU**

\_\_\_\_\_

Assoc. Prof. Dr. Alpan BEK  
Supervisor, **Physics Dept., METU**

\_\_\_\_\_

**Examining Committee Members:**

Prof. Dr. Mehmet Parlak  
Physics Dept., METU

\_\_\_\_\_

Assoc. Prof. Dr. Alpan Bek  
Physics Dept., METU

\_\_\_\_\_

Assoc. Prof. Dr. M. Emre Taşgın  
Institute of Nuclear Sciences, Hacettepe Univeristy

\_\_\_\_\_

Assoc. Prof. Serhat Çakır  
Physics Dept., METU

\_\_\_\_\_

Assoc. Prof. Dr. H. Emrah Ünalın  
Metallurgical and Materials Engineering Dept., METU

\_\_\_\_\_

**Date:**

*27.01.2017*

**I hereby declare that all information in this document has been obtained and presented in accordance with academic rules and ethical conduct. I also declare that, as required by these rules and conduct, I have fully cited and referenced all material and results that are not original to this work.**

Name, Last name: Gizem Birant

Signature:

## ABSTRACT

### **SURFACE COVERAGE CONTROL OF SELF ORGANIZED PLASMONIC NANOSTRUCTURES AT INTERFACES OF PHOTOVOLTAICS RELATED MATERIALS**

Birant, Gizem

M. Sc. Department of Physics

Supervisor: Assist. Prof. Dr. Alpan Bek

January 2017, 87 pages

In this thesis, it has been demonstrated that light management in photovoltaic devices might be achieved via plasmonic interfaces. New strategies have been developed to achieve a 10% surface coverage ratio that is ideal for light management. First, metal nanoparticles are synthesized as colloidal solutions. Metal nanoparticles are preferred because when they are coated on the surface of the solar cell, they increase the optical path length of the light in the cell via interacting and scattering the incident light. In this study, silver nanoparticles have been chosen considering their strong resonance characteristics and their low cost compared to gold. The industrial scale solar cells with surface roughness due to saw damage etching are coated with colloidal silver nanoparticle solution by a spray gun. Then heat treatment is applied on these surfaces to form the plasmonic interfaces. In order to examine the localized surface plasmon resonance properties of silver nanoparticles, silicon solar cells are produced in three different thickness levels of silicon nitride ( $Si_3N_4$ ). Then, the nanoparticle solution is spray coated by different numbers of passes on the aforementioned silicon solar cells with different thickness levels. Via this study, the effect of the number of spray passes on localized surface plasmon resonance is observed. After the spray coating step, the specular reflectance, diffuse reflectance, haze and quantum efficiency measurements

are made. The optical and electrical properties of the nanoparticles are determined by these measurements. With the aid of a solar simulator, improvements in the efficiencies of full-scale solar cells are identified. As a result of the spray coating method, it has been observed that the increase in efficiency of the solar cells depend both on the number of spray passes and on the structure of the solar cells used. By developing this study, the efficiencies of full-scale silicon solar cells can be increased beyond the known limits by also controlling the production steps of the cells. In this context, this work can be used as a roadmap.

**Keywords:** Metal Nanoparticles, Plasmonic Interfaces, Surface Coverage Control, Solar Cells, Colloidal Nanoparticle Synthesis, Efficiency Increase

## ÖZ

# FOTOVOLTAİK MALZEMELERİN ARAYÜZLERİNİN KENDİLİĞİNDEN OLUŞUMLU PLAZMONİK NANO YAPILARLA KONTROLLÜ ORANDA KAPLANMASI

Birant, Gizem

Yüksek Lisans, Fizik Bölümü

Tez Yöneticisi: Doç. Dr. Alpan Bek

Ocak 2017, 87 sayfa

Bu tez çalışmasında fotovoltaik aygıtlarda ışık yönetiminin plazmonik ara yüzlerle gerçekleştirilebileceği gösterilmiştir. Işık yönetimi için ideal olan %10 yüzey kaplanma oranını elde etmek için yeni stratejiler geliştirilmiştir. Öncelikle metal nano parçacıklar koloidal çözelti olarak sentezlenmiştir. Metal nanoparçacıkların tercih edilme sebebi güneş gözelerinin yüzeyine kaplandıkları takdirde güneşten gelen ışıkla etkileşime geçip ışığın saçılmasını sağlayarak göze içerisindeki optik yol uzunluğunu arttırmalarıdır. Bu çalışmada sahip olduğu güçlü rezonans özelliği ve altına oranla maliyet olarak uygunluğu göz önünde bulundurularak gümüş nanoparçacıklar tercih edilmiştir. Tam boyutta, testere hasarlandırmasına bağlı yüzey pürüzlülüğü bulunan, silisyum güneş gözelerinin yüzeyleri koloidal olarak sentezlenen gümüş nanoparçacık çözeltisi ile spreyle kaplama tekniği aracılığıyla kaplanmıştır. Daha sonra bu yüzeylere ısı işlem uygulanarak gümüş nanoparçacıkların plazmonik ara yüz oluşturması sağlanmıştır. Gümüş nanoparçacıkların yerel plazmon salınım özelliklerini inceleyebilmek adına silisyum güneş gözeleri üç farklı silisyum nitrür ( $Si_3N_4$ ) kalınlığında üretilmiştir. Daha sonra nanoparçacık çözeltisi değişik silisyum nitrür kalınlığındaki gözelerle farklı geçiş sayılarında püskürtülmüş, geçiş sayısının da yerel plazmon salınımına etkisi incelenmiştir. Spreyle kaplama aşamasından sonra gözelerin yansıtma, yayınlık yansıtma, pus ve kuantum verimlilik ölçümleri yapılmıştır. Bu

ölçümler sayesinde nanoparçacıkların optik özellikleri belirlenmiştir. Solar simülatör yardımıyla da tam boyuttaki güneş gözelerinin etkinliklerindeki iyileştirmeler tespit edilmiştir. Spreyle kaplama yöntemi sonucunda etkinlik artışının hem spreyle geçiş sayısına hem de kullanılan gözenin yapısına bağlı olduğu gözlemlenmiştir. Bu çalışma geliştirilerek tam boyuttaki silisyum güneş gözelerinin etkinlikleri üretim aşamaları da kontrol edilerek bilinen limitlerin üzerine çıkarılabilir. Bu bağlamda bu çalışma bir yol haritası olarak kullanılabilir.

**Anahtar Kelimeler:** Metal Nanoparçacıklar, Plazmonik Ara yüzler, Kontrollü Yüzey Kaplaması, Güneş Gözesi, Koloidal Nanoparçacık Sentezi, Verim Artışı,

*To my beloved family..*

## ACKNOWLEDGEMENTS

I offer my first and most sincere gratitude to my advisor Assoc. Prof. Dr. Alpan BEK for his immense knowledge, patience and support. Without his guidance, I would not be able to finish my M.Sc. in Physics and complete my studies related to this thesis. I would like to thank him again for responding to all of my endless questions, and motivating me all the time I need.

I would like to thank Prof. Dr. Raşit Turan for allowing me to use the equipment in the laboratories of the GÜNAM facility. I also thank all the members of the GÜNAM for their support.

I also would like to thank Assoc. Prof. Dr. Emrah Ünalan and his team for their help and letting me to use their laboratory.

I am grateful to thank Özge Demirtaş, M. Kurtuluş Abak, Mete Günöven, Ezgi Aygün and the rest of our Nano-Optics Group members. It is a chance for me to work with them all. It was almost impossible for me to finish this work without their support.

I kindly acknowledge financial support from TÜBİTAK under project no: 113M931

Finally, I would like to express my endless love and thank to my dearest family for supporting and believing me all the time. Without their help, I could not be the person I am right now.

My last thank is for the person who is physically farthest but closest to me all the time..

## TABLE OF CONTENTS

ABSTRACT.....	v
ÖZ .....	vii
ACKNOWLEDGMENTS .....	x
TABLE OF CONTENTS.....	xi
LIST OF TABLES .....	xiii
LIST OF FIGURES .....	xiv
LIST OF ABBREVIATIONS .....	xix

### CHAPTERS

1. INTRODUCTION .....	1
2. BRIEF INTRODUCTION TO PV TECHNOLOGY .....	3
2.1 Types of Solar Cells .....	3
2.1.1 1 <sup>st</sup> generation solar cells .....	3
2.1.2 2 <sup>nd</sup> generation solar cells .....	4
2.1.3 3 <sup>rd</sup> generation solar cells.....	4
2.2 Photovoltaics .....	5
2.2.1 p-n junction .....	5
2.2.2 Built-in electric field for crystalline silicon solar cells .....	5
2.3 Photovoltaic Effect.....	6
2.4 Characteristics of PV.....	6
2.5 Solar Irradiation .....	10
2.6 Bandgap Energy .....	12
2.7 The Shockley–Queisser limit .....	12
2.8 PV Market .....	13
3. PLASMONICS PRINCIPLES .....	15
3.1 Bulk Plasmons.....	15
3.2 Surface Plasmon Polaritons (SPPs).....	16
3.3 Localized Surface Plasmon Polaritons (LSPR).....	17
3.3.1 Localized Surface Plasmon Resonance Mechanisms .....	18
3.4 Is It Possible to Exceed Shockley-Queisser Limit by LSPR?.....	20
3.5 Efficiency Enhancement by LSPR in Solar Cells .....	20
4. EXPERIMENTAL METHODS .....	24
4.1 Production of mono-crystalline silicon solar cell.....	23
4.2 Polyol Synthesis of Silver Nanoparticles.....	25
4.2.1 Procedure.....	25
4.2.2 Purification part.....	26
4.3 Spray Coating Technique .....	27
4.4 Optical Characterization.....	28
4.4.1 Reflection Set-Up.....	28
4.5 Electrical Characterization .....	30
4.5.1 I-V Measurements .....	30
4.5.2 Quantum Efficiency Set-up.....	31

4.6	Image Analysis Method .....	32
4.6.1	Example Analysis.....	32
5.	RESULTS AND DISCUSSION .....	35
5.1	Reflection Measurements Results:.....	39
5.1.1	Reflection graphs of SET 1 (5-10 nm Silicon Nitride) .....	39
5.1.2	Reflection Graphs of SET 2 (10-15nm Silicon Nitride) .....	41
5.1.3	Reflection Graphs of SET 3 (18-20 nm Silicon Nitride) .....	42
5.2	Diffuse Reflection Measurements Results .....	44
5.2.1	Diffuse Reflection Graphs of SET 1 (5-10 nm Silicon Nitride) .....	44
5.2.2	Diffuse Reflection Graphs of SET 2 (10-15 nm Silicon Nitride) .....	46
5.2.3	Diffuse Reflection Graphs of SET 3 (18-20 nm Silicon Nitride) .....	47
5.3	SEM Imaging Analysis .....	49
5.3.1	SEM Images for SET 1 .....	49
5.3.2	SEM Images for SET 2 .....	51
5.3.3	SEM Images for SET 3 .....	54
5.4	Solar Simulator Measurement Results .....	56
5.4.1	Current- Voltage Graphs of SET 1 .....	57
5.4.2	Current- Voltage Graphs of SET 2.....	58
5.4.3	Current- Voltage Graphs of SET 3.....	59
5.4.4	Efficiency, Short Circuit Current ( <i>I<sub>sc</sub></i> ), Open Circuit Voltage ( <i>V<sub>oc</sub></i> ) and Fill Factor (FF) Values; before and after spray coating process .....	60
5.5	Comparison of the Sets .....	64
5.5.1	Relation between surface coverage rates and the number of spray passes for all sets .....	65
5.5.2	Relation between increase in efficiency and surface coverage for all sets	67
5.5.3	Reflection, Diffuse Reflection and Haze Analysis for all sets .....	69
5.6	Quantum Efficiency Measurement Results.....	76
5.7	The “125” case .....	81
	CONCLUSIONS.....	83
	REFERENCES.....	85

## LIST OF TABLES

### TABLES

Table-1 Increase in $\eta$ and change in F.F., $V_{oc}$ and $I_{sc}$ of SET 1.....	62
Table-2 Increase in $\eta$ and change in F.F., $V_{oc}$ and $I_{sc}$ of SET 2.....	64
Table-3 Increase in $\eta$ and change in F.F., $V_{oc}$ and $I_{sc}$ of SET 3.....	65

## LIST OF FIGURES

### FIGURES

Figure 1.1 a- SEM image of silicon solar cell with 10nm Ag NP formed by dewetting technique b- Change in efficiency table.....	2
Figure 2.1 Poly- and Mono- Crystalline Silicon Solar Cells.....	3
Figure 2.2 Photo of CdTe Thin Film Solar Cell.....	4
Figure 2.3 Photo of Organic Solar Cell .....	4
Figure 2.4 Solar Cell Representation .....	5
Figure 2.5 p-n junction under illuminated light .....	6
Figure 2.6 IV curves of dark and illuminated diodes .....	7
Figure 2.7 IV and PV Curves for showing the basic characteristics of the cell.....	8
Figure 2.8 Interpreting Fill Factor by I-V Curve .....	9
Figure 2.9 AM 1.5 Spectrum .....	11
Figure 2.10 a-Representation of AM 1.5 Spectrum and Zenith Angle b-Direct and Global Radiation .....	11
Figure 2.11 Bandgap Energies of Different Semiconductor Materials and Shockley-Queisser Limit .....	12
Figure 2.12 Global Weighted Average Total System Costs Breakdown of Utility-Scale PV Systems, 2009-2025 .....	13
Figure 2.13 Annual PV Production by Technology – Worldwide (in GWp) .....	14
Figure 3.1 Frequency dependence of Bulk Plasmons .....	16
Figure 3.2 Propagating charge waves caused by electron oscillations known as SPPs .....	16
Figure 3.3 Absorption and scattering cross-section caused by LSPR .....	17
Figure 3.4 Schematic illustration of the importance of the size of a nanoparticle for its plasmonic enhancement mechanism .....	18
Figure 3.5 Schematic illustration of plasmon enhancement mechanisms of radiative effects .....	19
Figure 3.6 Scattering light from metal nanoparticles .....	20

Figure 3.6 Fraction of light scattered into substrate for Ag nanoparticles on a 10nm thick silicon dioxide under layer on silicon .....	21
Figure 3.7 Maximum path length enhancement for the geometries in Figure 2.6 at a wavelength of 800nm .....	22
Figure 3.8 Angular distribution of scattered power for a parallel dielectric dipole that is 10 nm above a silicon surface and Lambertian scatterer .....	22
Figure 4.1 Fabrication process of silicon mono-crystalline solar cell .....	24
Figure 4.2: Color Scale of Nitride Thickness on Solar Cell .....	25
Figure 4.3 Photo of AgNPs Synthesis Setup.....	27
Figure 4.4 Photo of 1, 2 and 3; Synthesized AgNPs solutions without purification and 4; AgNPs in ethanol .....	28
Figure 4.5 Photo of Spray Coating Technique .....	28
Figure 4.6 Schematic of Reflection Measurement Set-up .....	29
Figure 4.7 Types of Reflection .....	30
Figure 4.8 Schematic drawing of I-V Measurement Set-up .....	31
Figure 4.9 Schematic of Quantum Efficiency Set-up .....	32
Figure 4.10 Schematic Representation of Image Analyzing Procedure .....	34
Figure 5.1 Surface Coverage vs. Number of spray passes graph of aforementioned study with flat silicon wafers .....	38
Figure 5.2 Laser Cut Set-Up .....	39
Figure 5.3 Sketch of laser cut process .....	39
Figure 5.4 Reflectance Graph of A for SET 1 .....	41
Figure 5.5 Reflectance Graph of B for SET 1 .....	42
Figure 5.6 Reflectance Graph of C for SET 1 .....	42
Figure 5.7 Reflectance Graph of A for SET 2 .....	43
Figure 5.8 Reflectance Graph of B for SET 2 .....	43
Figure 5.9 Reflectance Graph of C for SET 2 .....	44
Figure 5.10 Reflectance Graph of A for SET 3 .....	44
Figure 5.11 Reflectance Graph of B for SET 3 .....	45
Figure 5.12 Reflectance Graph of C for SET 3 .....	45
Figure 5.13 Diffuse Reflectance Graph of A for SET 1 .....	46
Figure 5.14 Diffuse Reflectance Graph of B for SET 1 .....	47

Figure 5.15 Diffuse Reflectance Graph of C for SET 1 .....	47
Figure 5.16 Diffuse Reflectance Graph of A for SET 2 .....	48
Figure 5.17 Diffuse Reflectance Graph of B for SET 2 .....	48
Figure 5.18 Diffuse Reflectance Graph of C for SET 2 .....	49
Figure 5.19 Diffuse Reflectance Graph of A for SET 3 .....	49
Figure 5.20 Diffuse Reflectance Graph of B for SET 3 .....	50
Figure 5.21 Diffuse Reflectance Graph of C for SET 3 .....	50
Figure 5.22 SEM image of the reference (uncoated) device of SET 1 named 100A .....	51
Figure 5.23 SEM image of the reference (uncoated) device (100A) with 75° tilt. ....	52
Figure 5.24 SEM images of SET 1 .....	52
Figure 5.25 SEM image of the reference (uncoated) device of SET 2 named 200A .....	53
Figure 5.26 SEM image of the reference (uncoated) device (200A) with 75° tilt. ....	54
Figure 5.27 SEM image of the sample named 220A .....	54
Figure 5.28 SEM images of SET 2 .....	55
Figure 5.29 SEM image of the reference (uncoated) device of SET 3 named 300A .....	56
Figure 5.30 SEM image of the reference (uncoated) device (300A) with 75° tilt. ....	56
Figure 5.31 SEM images of SET 3 .....	57
Figure 5.32 Schematic Representation of Current-Voltage (I-V) Curve .....	58
Figure 5.33 Current-Voltage (I-V) Graphs of SET 1 before and after coating .....	59
Figure 5.34 Current-Voltage (I-V) Graphs of SET 2 before and after coating .....	60
Figure 5.35 Current-Voltage (I-V) Graphs of SET 3 before and after coating .....	61
Figure 5.36 Nanoparticles plasmonic behaviors with changing diameter .....	63
Figure 5.37 Schematic of Localized Surface Plasmon Resonance .....	64
Figure 5.38 Schematic of the reading a box chart .....	66
Figure 5.39 Surface coverage (%) vs. Number of Spray Passes for SET 1 .....	67
Figure 5.40 Surface coverage (%) vs. Number of Spray Passes for SET 2 .....	68
Figure 5.41 Surface coverage (%) vs. Number of Spray Passes for SET 3 .....	68
Figure 5.42 Increase in efficiency (%) vs. Surface Coverage (%) for SET 1 .....	69
Figure 5.43 Increase in efficiency (%) vs. Surface Coverage (%) for SET 2 .....	70

Figure 5.44 Increase in efficiency (%) vs. Surface Coverage (%) for SET 3 .....	71
Figure 5.45 Integral Reflectance values over 400-1000nm Spectral Range vs. Sample Position & Number of Spray Passes for SET1 .....	72
Figure 5.46 Integral Reflectance values over 400-1000nm Spectral Range vs. Sample Position & Number of Spray Passes for SET2 .....	72
Figure 5.47 Integral Reflectance values over 400-1000nm Spectral Range vs. Sample Position & Number of Spray Passes for SET3 .....	73
Figure 5.48 Integral Diffuse reflectance values over 400-1000nm Spectral Range vs. Sample Position & Number of Spray Passes for SET1 .....	74
Figure 5.49 Integral Diffuse reflectance values over 400-1000nm Spectral Range vs. Sample Position & Number of Spray Passes for SET2 .....	74
Figure 5.50 Integral Diffuse reflectance values over 400-1000nm Spectral Range vs. Sample Position & Number of Spray Passes for SET3 .....	75
Figure 5.51 Integral Haze values (%) over 400-1000nm Spectral Range vs. Sample Position & Number of Spray Passes for SET1 .....	76
Figure 5.52 Integral Haze values (%) over 400-1000nm Spectral Range vs. Sample Position & Number of Spray Passes for SET2 .....	76
Figure 5.53 Integral Haze values (%) over 400-1000nm Spectral Range vs. Sample Position & Number of Spray Passes for SET3 .....	77
Figure 5.54 Integral External Quantum Efficiency Values over 400-1000nm Spectral Range vs. Sample Position & Number of Spray Passes for SET1 .....	79
Figure 5.55 Integral Internal Quantum Efficiency Values over 400-1000nm Spectral Range vs. Sample Position & Number of Spray Passes for SET1 .....	79
Figure 5.56 Integral External Quantum Efficiency Values over 400-1000nm Spectral Range vs. Sample Position & Number of Spray Passes for SET2 .....	80
Figure 5.57 Integral Internal Quantum Efficiency Values over 400-1000nm Spectral Range vs. Sample Position & Number of Spray Passes for SET2 .....	80
Figure 5.58 Integral External Quantum Efficiency Values over 400-1000nm Spectral Range vs. Sample Position & Number of Spray Passes for SET3 .....	81

Figure 5.59 Integral Internal Quantum Efficiency Values over 400-1000nm  
Spectral Range vs. Sample Position & Number of Spray Passes for SET3 .....81  
Figure 5.60 SEM image of the sample named 125 .....83

## LIST OF ABBREVIATIONS

### ABBREVIATIONS:

EQE	External Quantum Efficiency
IQE	Internal Quantum Efficiency
LSPR	Localized Surface Plasmon Resonance
MNP	Metal Nanoparticle
SEM	Scanning Probe Microscopy
SPP	Surface Plasmon Polariton



## CHAPTER 1

### INTRODUCTION

In this study, new strategies have been developed to coat about 10% of silicon (Si) solar cell surfaces with silver (Ag) nanoparticles. First, Ag nanoparticles were synthesized as a colloidal solution and the surfaces of the Si solar cells, with different silicon nitride ( $Si_3N_4$ ) thicknesses, were coated at controlled amounts using the spray coating technique. Then these surfaces were heat treated to form plasmonic interfaces. The top surface was coated in a suitable manner, resulting in an efficiency increase of  $6 \pm 2\%$ .

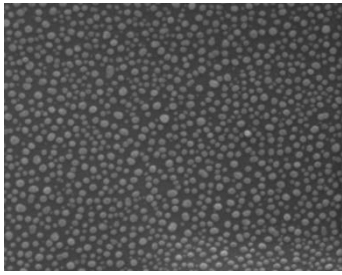
The reason for creating a plasmonic interface in solar cells is that they can provide an increase in efficiency of solar cells that have not yet passed 20% band. With better photon management, this 20 percent rate can be brought to higher values.

When it comes to the efficiency of solar cells, Shockley-Queisser Limit comes into play. This limit predicts the maximum solar cell efficiency to be around 33.7%. [1]

Yablonovitch on the other hand, shows that theoretically the efficiency of any solar cell can be increased by up to  $4n^2$  using photonics, where  $n$  is the refractive index. [2] Yet the efficiencies of silicone solar cells produced with routine techniques has not exceeded 20%.

A number of improvements with plasmonics have been proposed, besides photonic concepts, to exceed the Yablonovitch limit.

In this context, recent study, which is “Self-organized fabrication” (dewetting technique), is a very suitable strategy for production of large area plasmonic interfaces. However for that work the surface coverage of plasmonic structures lies around 25-35% on interfaces. [3] This is too high with respect to the ideal value of 10% for the optimum light management. [4]



**a**

Device	Cell Efficiency (%)
10 nm bare flat	11.02
10 nm Ag NP flat	10.9

**b**

**Figure 1.1** a- SEM image of silicon solar cell with 10nm Ag NP formed by dewetting technique b- change in efficiency table [3].

As can be seen from the Figure 1.1, surface coverage around 30% caused decrease in efficiency of solar cell.

Another reason why this work cannot be applied on the routine silicon solar cell production is that it is very expensive to apply in large areas. The method used for constructing plasmonic interfaces should be cost-effective, like in this thesis.

This thesis explains how silver nanoparticles are coated on silicon solar cell surfaces in controlled amounts by spray coating technique. Three set of silicon solar cells with three different silicon nitride ( $Si_3N_4$ ) thicknesses (5-10nm, 10-15nm and 18-20nm) were examined to identify the relationship between the plasmonic effects and the silicon nitride thickness. This technique provided a surface coverage of 6.42% on average, independent of the silicon nitride thicknesses. As already mentioned, the efficiency of full scale solar cells has been increased by  $6\pm 2\%$  with created plasmonic interfaces. The principles of plasmonics related to this thesis will be given in the following chapters. There is also statistical analysis of optical and electrical measurements results via box charts at results and discussion part.

Also, a brief section related to the features and working principles of the photovoltaic devices will be shared in order to better understand the photovoltaic based motivation of this work.

## CHAPTER 2

### BRIEF INTRODUCTION TO PV TECHNOLOGY

Devices which convert sunlight directly into electricity are called solar cells. We can consider solar cells as two terminal devices which conduct like diode in the dark but generate a photo voltage when charged by the sun. [5] Nearly all solar cells are made of semiconductor materials that can absorb solar radiation. It is a thin slice of semiconductor material around 169 cm<sup>2</sup> in area. [6]

#### 2.1 Types of Solar Cells:

Solar cells are classified in three generations.

##### 2.1.1 1<sup>st</sup> generation solar cells:

Solar cell which are produced on silicon wafers are called 1<sup>st</sup> generation solar cells. This generation is also known as the oldest and because of the high efficiency values the most commonly used technology. For further categorization, the silicon wafer based technology is divided into two subgroups named as;

- Single/ Mono-crystalline silicon solar cell.
- Poly/Multi-crystalline silicon solar cell. [7]

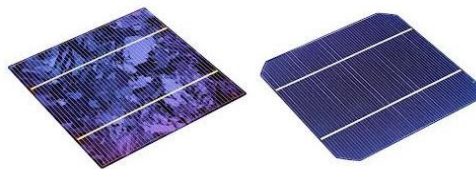


*Figure 2.1 Poly- and mono- crystalline silicon solar cells [8].*

### 2.1.2 2<sup>nd</sup> generation solar cells:

Most of the thin film solar cells are known as 2<sup>nd</sup> generation solar cells. These cells are cost-effective in comparison to 1st generation solar cells. One can be categorized thin film solar cells as:

- a-Si.
- CdTe.
- CIGS (copper indium gallium di-selenide).

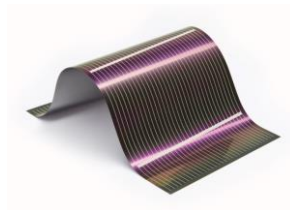


*Figure 2.2 Photo of CdTe thin film solar cell [9].*

### 2.1.3 3<sup>rd</sup> generation solar cells:

The new promising technologies in solar cell production is called as 3<sup>rd</sup> generation. These technologies are mostly not investigated in detail. Some of the novel technologies are:

- Nano crystal based solar cells.
- Polymer based solar cells.
- Dye sensitized solar cells.
- Organic solar cells.

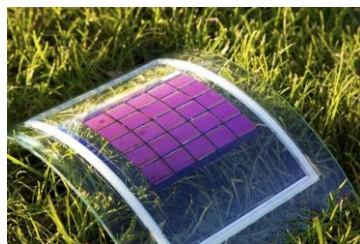


*Figure 2.3 Photo of an organic solar cell [10].*

## 2.2 Photovoltaics:

Solar cell in the dark is acting like a simple diode which is produced by the combination of p and n type semiconductors. In the dark the solar cell in Figure 2.4 does nothing. When it is switched on by the light it develops a voltage and then current drawn. [5]

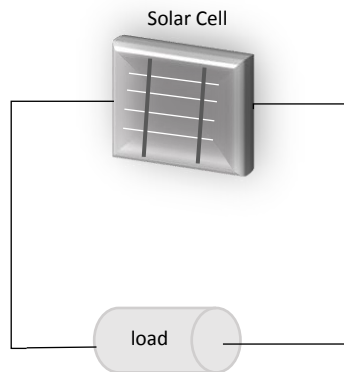


*Figure 2.4 Solar Cell Representation [5].*

It would be more accurate to tell what the p-n junction is before the characteristics of the photovoltaic devices are described.

### 2.2.1 p-n junction:

One side of the silicon is doped with boron (p-type) and the other side is doped with phosphorus (n-type) to form a p-n junction. The n-type material has greater number of free moving electrons (negatively charged) and for balancing the free electrons there are number of not moving positive ions. Similarly, the p-type material has the large numbers of moving free holes (positively charged) and again to balance the positive ions there are negative ions that are not moving freely. [11]

### 2.2.2 Built-in electric field for crystalline silicon solar cells:

When n-type and p-type materials are brought together, electrons from n-type side start to diffuse into p-type side. The major reason for diffusion is the excess number of mobile electrons on n-type side due to doping process. Similar condition is valid for p-type side. Due to the doping process there are large number of mobile holes on p-type side and they start to diffuse into n-type side. [11]

In diffusion process, both mobile electrons and holes leave behind fixed ions. For n-type side they are phosphorous ions and for p-type side boron ions. When mobile electrons and holes cross the junction, the fixed ions that left behind establish a “built-in” electric field at the junction. Therefore, electrons and holes start to flow in opposite direction to the flow caused by diffusion because of this establishing “built-in” electric field.

This separation of charge creates an electric field at the junction which is in opposition to that already existing at the junction.[11]

**2.3 Photovoltaic Effect:**

A positive voltage is applied to the p-type side and a negative voltage to the n-type side for current to flow. The built-in electric field and applied electric field are in opposite direction at p-n junction as seen in Figure 2.5. [11]

The collection of light-generated carriers by the p-n junction causes a movement of electrons to the n-type side and holes to the p-type side of the junction. This is called photovoltaic effect.

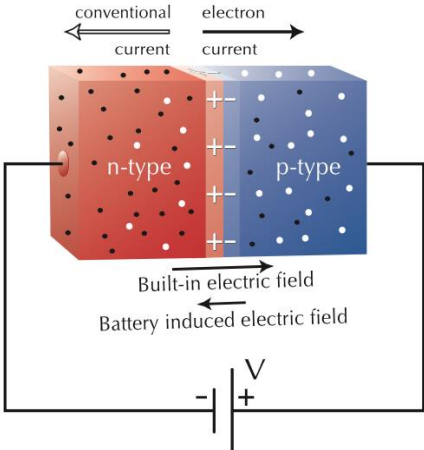


*Figure 2.5 p-n junction under illuminated light [11].*

**2.4 Characteristics of PV:**

For an ideal solar cell, the corresponding I-V characteristics is explained by Shockley solar cell equation;

$$I = I_{ph} - I_0(e^{\frac{qV}{k_B T}} - 1) \tag{2.1}$$

Here  $k_B$  is the Boltzmann constant,  $T$  is the absolute temperature,  $V$  is the voltage between terminals,  $q$  is the electron charge,  $I_0$  is the diode saturation current and  $I_{ph}$  is the photocurrent.

The “ $I_0$ ” is the most important parameter in diodes. It differentiates the one diode from another. The recombination of the solar cell is measured by  $I_0$  itself. The larger recombination means the highest  $I_0$  [6].

The photocurrent ( $I_{ph}$ ) which is generated under illumination by the solar cell on the other hand is related to photon flux incident on the cell and is dependent on the incident light. [12] It is independent of the applied voltage.

The corresponding I-V curves, dark and illuminated, are given in Figure 2.6.

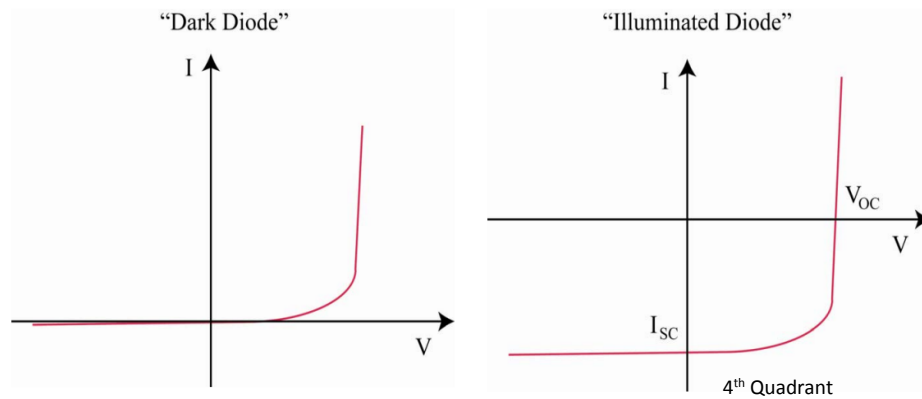


**Figure 2.6** *IV curves of dark and illuminated diodes.*

In order to obtain conventional I-V curve, the 4<sup>th</sup> quadrant is taking into account and the curve is mirrored. The basic electrical characteristics of the solar cells are open circuit voltage ( $V_{oc}$ ), short circuit current ( $J_{sc}$ ), fill factor (FF), efficiency ( $\eta$ ), series resistance ( $R_s$ ), shunt resistance ( $R_{sh}$ ), maximum power point, maximum power voltage ( $V_{mp}$ ) and maximum power current ( $J_{mp}$ ).

All of these characteristics/parameters can be derived from IV curve. (Figure 2.7)

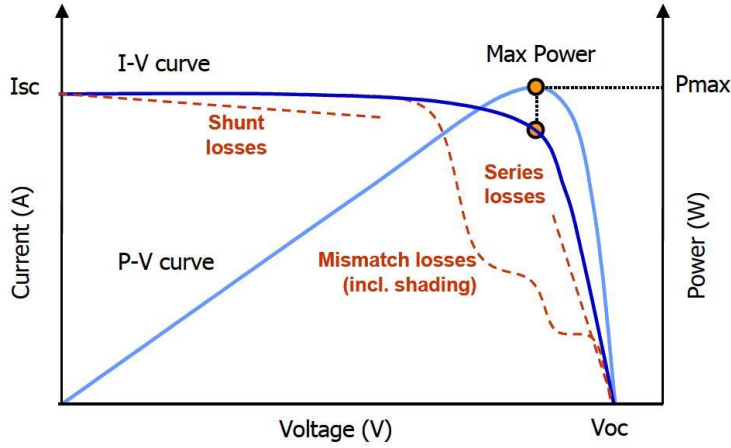


**Figure 2.7** IV and PV Curves for showing the basic characteristics of the cell [13].

- **Quantum Efficiency:**

The probability that an incident photon of energy  $E$  will deliver one electron to the external circuit is the cell's quantum efficiency. It is possible to define external and internal quantum efficiencies. ( $EQE$  &  $IQE$  respectively) The difference between them is in the treatment of reflected photons from the cell; if all the photons that hit on the surface of the cell are considered, it gives the value of external quantum efficiency. But if only the photons that are not reflected are considered, they are giving the value of internal quantum efficiency. [5] [12]

$$EQE(\lambda) = \frac{\text{electron count}}{\text{photon count}} \quad (2.2)$$

$$IQE(\lambda) = \frac{EQE(\lambda)}{1-R(\lambda)} \quad (2.3)$$

- **Short Circuit Current (Photocurrent):**

For ideal cases, the photocurrent is equal to short circuit current. ( $I_{sc}$ ) The short circuit current is also defined as the current through the cell when the cell is short circuited. It is also the largest current can be drawn from the cell. [6]

$$J_{sc} = q \int b_s(E)QE(E)dE \quad (2.4)$$

where;  $b_s(E)$  is the incident spectral photon flux density.

Short circuit current also be found from the intersection point of the I-V curve with vertical axes.

- **Open circuit voltage:**

When the contacts of the solar cell are isolated, that means there is no current flow, the value of the potential difference has its maximum, the open circuit value. [5] The value of the open circuit voltage can be detected from the intersection point of the I-V curve with horizontal axes. For mono crystalline solar cell, this value generally varies between 0.61-0.62 volts.

$$V_{oc} = \frac{n k T}{q} \ln\left(\frac{I_l}{I_0} + 1\right) \quad (2.5)$$

where  $I_l$  is the light generated current.

This equation shows that open circuit voltage not depends on short circuit current. The key effect is the saturation current  $I_0$ , and it depends on recombination of the cell. [6]

- **Maximum Power Point:**

Maximum power point of the solar cell is the highest value of the product of output voltage and output current ( $I \times V$ ) and can be determined from I-V curve. The values that gives the maximum power point is the maximum power voltage ( $V_{mp}$ ) and the maximum power current ( $J_{mp}$ ).

- **Fill Factor:**

Fill factor (FF) of the solar cell determines the maximum power from a cell. It is the ratio of maximum power point from the product of open circuit voltage and short circuit current. The FF is also showed the quality of the cell. [6] (Figure 2.8)

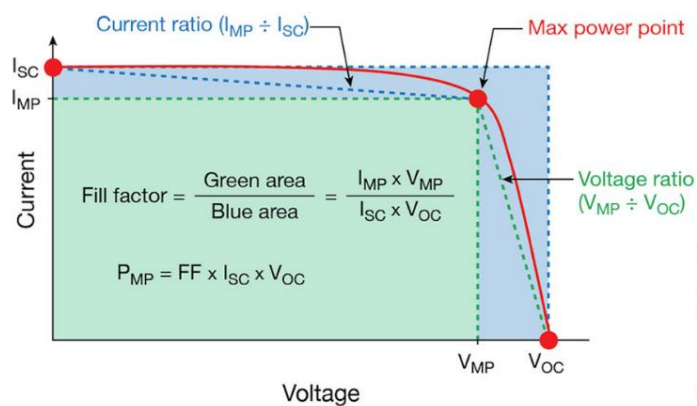


**Figure 2.8** Interpreting Fill Factor by I-V Curve [14].

$$FF(\%) = \frac{I_{mp}V_{mp}}{I_{sc}V_{oc}} = \frac{P_{max}}{P_T} \quad (2.6)$$

where  $P_T$  is the theoretical power of the cell.

- **Efficiency:**

The most basic definition of the efficiency is that efficiency is the ratio of the output energy from the cell to input energy from the sun. [6]

$$\eta = \frac{V_{oc}I_{sc}FF}{P_s} \quad (2.7)$$

where  $P_s$  is the input energy from the sun.

When solar cells are compared to each other, efficiencies of them are the most common characteristic for comparing.

- **Series Resistance:**

The series resistance can be defined as the resistance of the cell material to current flow from the resistive contacts. As can be seen from the Figure 2.7, series resistance can be calculated from IV graph. [5]

- **Shunt Resistance:**

This resistance is caused by leak currents through cell. This leakage is occurred for several reasons such as edge of the cells and problematic metallization or doping processes. Shunt resistance can also be calculated from IV curve. (Figure 2.7) [5]

## 2.5 Solar Irradiation:

$V_{oc}$ ,  $I_{sc}$ ,  $FF$  and  $\eta$  should be defined under certain illumination conditions for reasonable comparisons. The Standard Test Condition (STC) for solar cells is the Air Mass 1.5 spectrum, an incident power density of  $1000 \text{ W m}^{-2}$  with  $25 \text{ }^\circ\text{C}$ . (Figure 2.9) [5]

The AM 1.5 spectrum (so called “standard”) are used to detect PV cell performance measurements. Due to the fact that PV devices are selective in terms of spectra, there should be reference spectra for comparing the performance improvements. As said earlier according to American Society for Testing and Materials, the standard testing spectra is AM 1.5 spectra for both global and direct normal testing. [15]

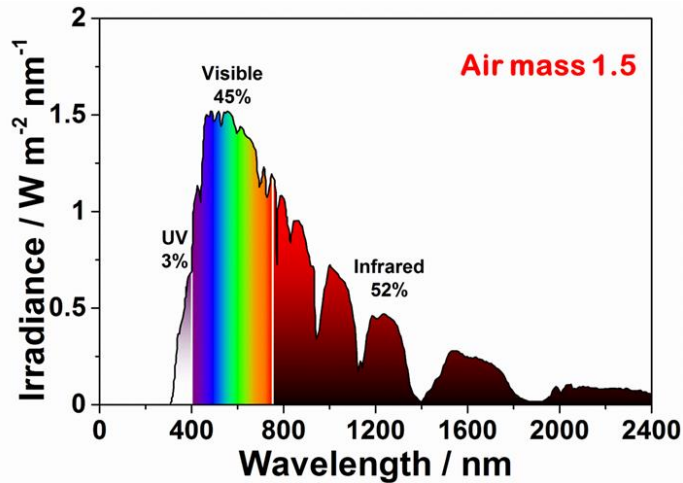


**Figure 2.9** AM 1.5 Spectrum [16].

The relative path length of the direct solar beam through the atmosphere is called air mass. The zenith angle ( $\theta_Z$ ) is increases, the air mass increases too. The zenith angle is used for standard testing is  $48.2^\circ$ , and the suffix 1.5 calculated according to this angle by following equation; (Figure 2.10 a)

$$AM = \frac{1}{\cos \theta_Z} \quad (2.7)$$

The irradiance including direct solar radiation from the sun’s disk plus sky and ground-reflected radiation incident on a cell is called “global”. “Direct” means the solar radiation from the sun’s disk plus forward-scattered radiation from around the disk (circumsolar). And normal refers to perpendicular rays coming from the sun to the device. (Figure 2.10 b) [15]

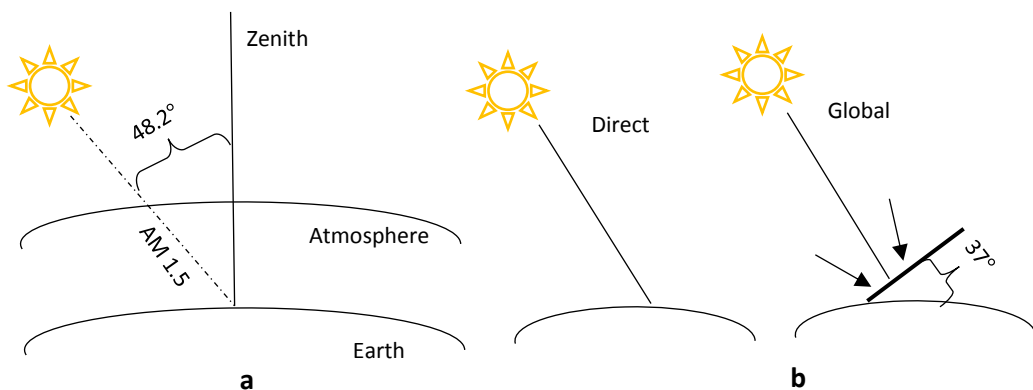


**Figure 2.10** a-Representation of AM 1.5 Spectrum and Zenith Angle b-Direct and Global Radiation

## 2.6 Bandgap Energy:

The amount of energy required to remove an electron from semiconductor's valance band and allow it to become a part of electrical circuit is called bandgap energy. [17] It is expressed in electron volts. (eV)

The energy of a photon must be at least as great as bandgap energy to free an electron. [17] The ones that have energy lower than bandgap escape unabsorbed but the ones that higher energies are absorbed but most of their extra energy expended as heat. [18]

The bandgap energy of crystalline silicon is 1.1 electron-volts. (eV) (Figure 2.11) On the other hand, the energy of light changes according to wavelengths of light. The energy spectrum of sunlight is in a range from 0.5 to 2.9 eV. (from infrared to ultraviolet) This means that nearly 55% of the energy of sunlight cannot be converted via PV cells because this energy is either below the bandgap of crystalline silicon or carries excess energy [17].

## 2.7 The Shockley–Queisser limit:

The Shockley-Queisser limit is the maximum theoretical efficiency of a solar cell with single p-n junction [1] (Figure 2.11).

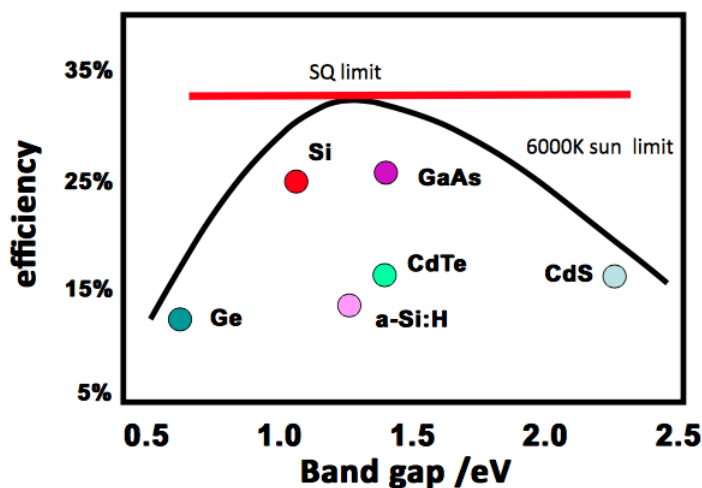


**Figure 2.11** Bandgap energies of different semiconductor materials and Shockley-Queisser limit [19].

This limit is calculated through the amount of electrical energy extracted per incident photon. In this calculation the bandgap energy of a single p-n junction is taken 1.4 eV (by using Am 1.5 Solar Spectrum) and then the maximum solar conversion efficiency is found around 33.7% [1].

## 2.8 PV Market:

Today one of the biggest problem of world is the energy. In order to meet today’s energy need, researchers are pursuing their tendencies towards clean and renewable energy sources like solar energy, wind, biomass or hydro energy because of the fact that fossil fuels are on the verge of extinction and cause severe pollution. [20] Among all types of renewable energies, the solar energy has an inexhaustible resource, the sun. The sun radiates more energy each day than the world uses in one year. But, the use of solar energy is much less than other types of energies, because of the production costs. In order to compete with other renewable energy sources, photovoltaic technology has to reduce production costs.

A general outline of the work done to reduce production costs is given in the graphic below. The decrease in costs from the past to today and the expected decrease trend in the years are seen in Figure 2.12.

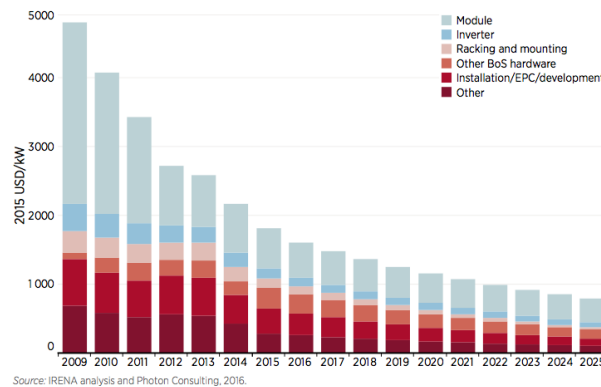


**Figure 2.12** Global Weighted Average Total System Costs Breakdown of Utility-Scale PV Systems, 2009-2025 [21].

According to “The Compound Annual Growth Rate” (CAGR) the PV installations was 42 % between 2000 and 2015. Si-wafer based PV technology accounted for about 93 % of the total production in 2015 by sharing the 68 % of total production with multi-

crystalline technology. In 2015, the market share of all thin film technologies amounted to about 8 % of the total annual production (Figure 2.13) [22].

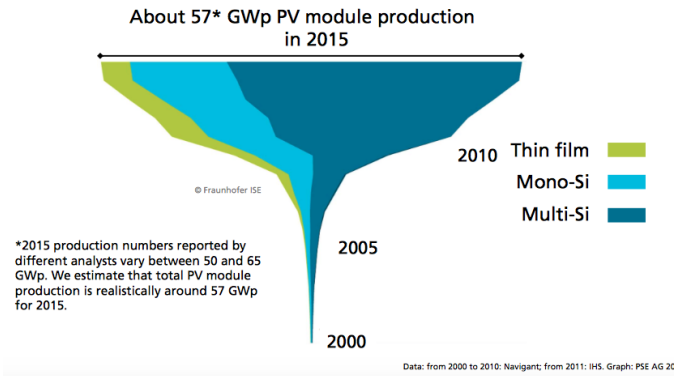


**Figure 2.13** Annual PV Production by Technology – Worldwide (in GWp) [22].

However, finding ways to increasing the efficiency of crystalline silicon solar cells is still a hot topic. Because silicon is an abundant and cheaper material. As said earlier the reduction of optical path length is the main reason of lower efficiencies. This problem can be solved by using nanoparticles, and plasmonic properties of metal nanoparticles. With this way light will be scattering into high angles, so the optical path length will increase. For minimizing the absorption losses in the metal, a plasmonic material with low losses in optical region should be chosen. [23]

## CHAPTER 3

### PLASMONICS PRINCIPLES

The investigation of optical phenomena associated with electromagnetic response of metals is called plasmonics or nanoplasmonics. This phenomena is mostly about the controlling of optical radiation on the subwavelength scale. [24]

The study of Plasmonics is a branch of nano-photonics. It studies how the electromagnetic (EM) field can be confined over a dimension of the order or smaller than the wavelength. Light causes the free electrons near the metal surface to be excited when it interacts with the metal nanoparticles. This interaction is hidden in the frequency dependence of the metals' complex dielectric function. [24]

Dielectric constant is a complex number and calculated by following equation:

$$\varepsilon = \varepsilon_1 + i\varepsilon_2 \quad (3.1)$$

$\varepsilon_1$  is the real part and represents the refraction of light, and  $\varepsilon_2$  is the imaginary part and describes the absorption.

Plasmonics can be examined under the following three headings;

#### 3.1 Bulk Plasmons:

Free electrons and ion cores in a bulk metal form a net neutrally charged plasma. Restoring force from the fixed ionic cores caused by local deviations in electron density leading to simple harmonic motion. [23]

The frequency of this motion can be found by following equation;

$$\omega_{BP} = \sqrt{\frac{n e^2}{m e_0}} \quad (3.2)$$

where  $e_0$  is permittivity of free space,  $n$  is the free electron density in solid,  $e$  is the electron charge and  $m$  is the effective mass of free electron

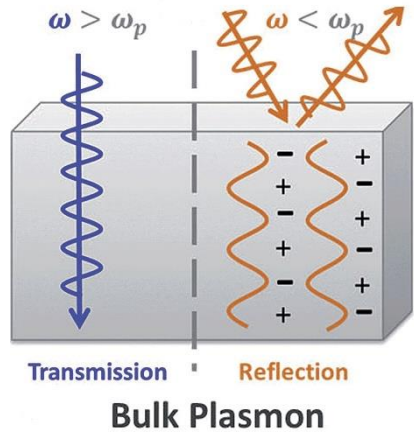


**Figure 3.1** Frequency dependence of Bulk Plasmons [25].

If the incoming light's frequency is higher than plasma frequency, (UV range for metals) the electrons will not oscillate. The light then will be absorbed or transmitted in interband transitions. [25] (Figure 3.1)

If the frequency of incoming light is smaller than the UV range, there is a strong reflection caused by electron oscillations  $180^\circ$  out of the phase with the incident light. [25]

**3.2 Surface Plasmon Polaritons (SPPs):**

If bulk metal is converted into a thin film, oscillations will only exist at the surface and cause the spread of charge waves known as "surface plasmon polaritons" (SPPs). [25]

This is a second type of electron density wave with transverse and longitudinal components on the metal surface. It happens at lower frequencies than frequency of bulk plasmon. [23] (Figure 3.2)

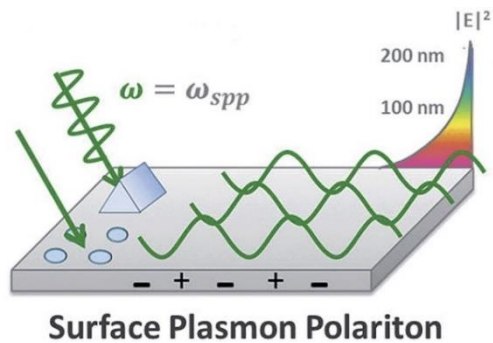


**Figure 3.2** Propagating charge waves caused by electron oscillations known as SPPs [25].

Derivation of Maxwell's equations gives the dispersion relation of SPPs;

$$k = \frac{\omega}{c} \left( \frac{\epsilon_1 \epsilon_2}{\epsilon_1 + \epsilon_2} \right) \quad (3.3)$$

where  $\epsilon_1, \epsilon_2$  the permittivities of the metal and dielectric either side of the surface. [23]

In the limit of large  $k$ , and using Drude model the frequency of surface plasmon polariton can be found by;

$$\omega_{SP} = \frac{\omega_{BP}}{\sqrt{2}} \quad (3.4)$$

### 3.3 Localized Surface Plasmon Polaritons (LSPR):

The restoring force is created by the standing wave of the electron density inside the particle, with surface charge. [23] This force leading to a characteristic oscillation frequency in the metal electrons like simple harmonic oscillation. This phenomenon is called localized surface plasmon resonance. (LSPR) [25] (Figure 3.3)

Localized surface plasmon resonances (LSPRs) are standing waves with zero net momentum. This means that there are no momentum matching conditions like SPPs. [23]

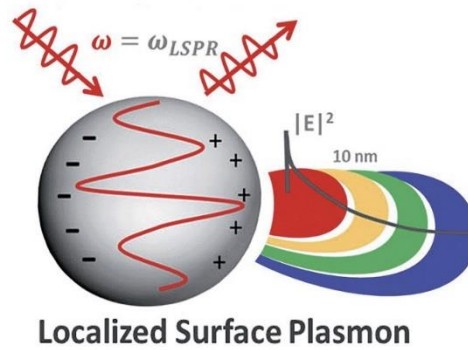


*Figure 3.3 Absorption and scattering cross-section caused by LSPR [25]*

All the electrons inside nanoparticle cannot push out by the radiation pressure of incoming light because they are held inside with much stronger force of lattice. [23]

The frequency of LSPR depends on polarization which can be found via;

$$\alpha = 4\pi\epsilon_0 r^3 \left( \frac{\epsilon_m - \epsilon_d}{\epsilon_m + 2\epsilon_d} \right) \quad (3.5)$$

where  $r$  is the radius of the sphere,  $\epsilon_m, \epsilon_d$  are the permittivities of the metal and the dielectric respectively. [23]

By assuming Drude form for the metallic permittivity and the surrounding dielectric vacuum, the result is;

$$W_{LSPR} = \frac{W_{BP}}{\sqrt{3}} \quad [23] \quad (3.6)$$

For LSPR only the particles larger than 10nm in diameter is taken into account because for smaller particles than this stronger quantum effects are shown. [23]

### 3.3.1 Localized Surface Plasmon Resonance Mechanisms:

Non-radiative damping by absorption caused by electron-phonon interactions, and/or radiative damping by the resonant scattering process can be seen after excitation of plasmon oscillations. [26] The size of the metal nanoparticles is important for the selection of the absorption and / or scattering procedures.

Particles smaller than 30 nm show only absorption while, the dominant procedure for particles around 50 nm is resonant scattering. at 50 nm both scattering and absorption exhibit but their spectral maxima are shifted relative the each other. When the particle size increases, the scattering becomes dominant. [26]

Metal nano-structures' radiative and non-radiative plasmonics properties are mainly controlled by their dimensions that strongly affect their light collecting ability as said earlier. [27]

This effect can be examined in detail at Figure 3.4:

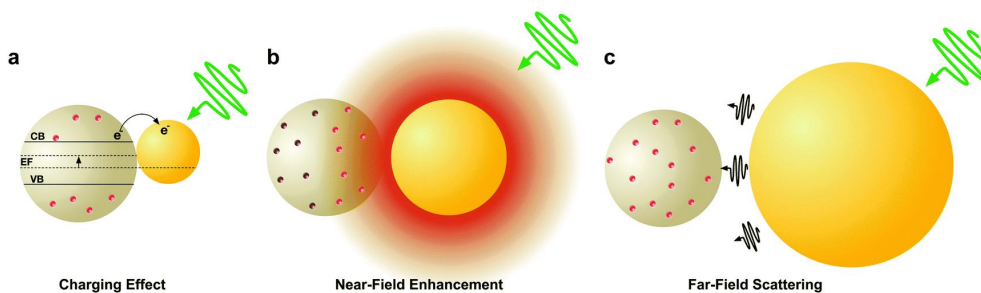


**Figure 3.4** Schematic illustration of the importance of the size of a nanoparticle for its plasmonic enhancement mechanism. a-) Photo charging effect from ~5 nm nanoparticle b-) Near-field plasmonic effect from a ~50 nm nanoparticle c-) light scattering as a result of ~100 nm nanoparticle [27].

In solar cells, plasmonic enhancement is provided by radiative and non-radiative effects of LSPR as said earlier.

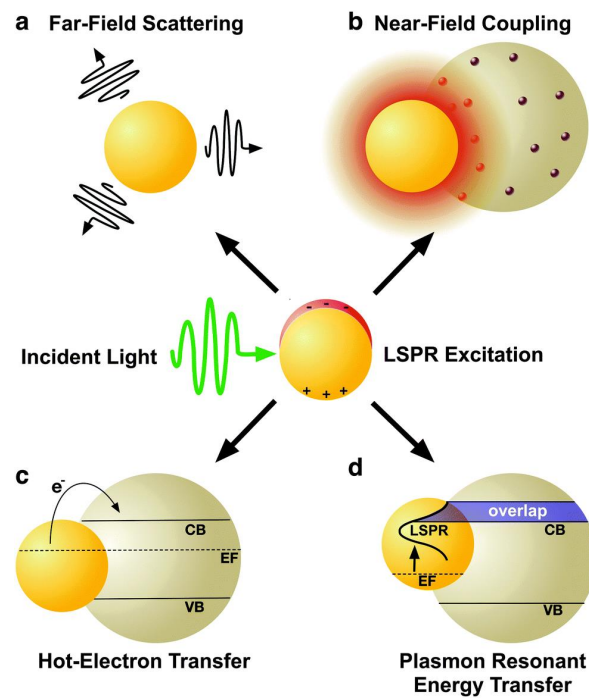


**Figure 3.5** Schematic illustration of plasmon enhancement mechanisms of radiative effects a-) far-field scattering and b-) near-field coupling; and non-radiative effects: c-) hot-electron transfer, and d-) plasmon resonant energy transfer [27].

LSPR's acting as a secondary light source that enhances the local electric fields by relaxes and then re-radiates light into the absorptive layer or the metal nano-structure, is named as radiative effects. Non-radiative effects on the other hand are seen when the LSPR transfers energy to neighboring semiconductors immediately after relaxation and increases current generation. During non-radiative processes, metal nano-structures act as a direct sensitizer. [27] The four mechanisms of plasmonic enhancement (radiative and non-radiative) are shown in Figure 3.5. Light scattering and electromagnetic fields are categorized as radiative effects. Hot electron transfer and plasmon resonant energy transfer are in non-radiative effects part.

### 3.4 Is It Possible to Exceed Shockley-Queisser Limit by LSPR?

S.-Q. Limit states that the maximum efficiency limit for solar cells is about 33.7%, as mentioned in section 1.1.6 of this thesis. When this limit calculated, only the near field effects of the particles are considered. However, as seen in Figure 3.4, particles also have far-field scattering effects. It can be said that this limit, also known as the Yablonovitch limit, can be exceeded if the far field scattering effects of the particles are added to the account. There are many studies in the literature showing that this limits exceeding.

### 3.5 Efficiency Enhancement by LSPR in Solar Cells:

Solar cells' surfaces are coated with thin silicon dioxide or silicon nitride layer for surface passivation as said in 4.1 section of the thesis. Because of this thin layer, particles that coated on the surface should be large enough to show themselves and their plasmonic properties. As mentioned in Figure 3.4, large particles as show dominantly scattering properties of LSPR.

As seen in the Figure 3.6, metal nanoparticles increase the optical path length of the light in the semiconductor by scattering the light. If there is no particle, light reflected back directly.

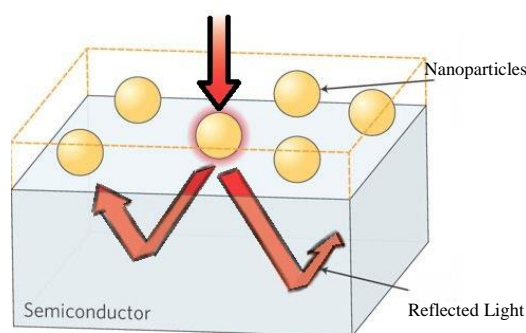


*Figure 3.6 Scattering light from metal nanoparticles [28].*

When it comes to increase the optical path length of the incident light in the solar cells, the most important factor is the fraction of light that is scattered into substrate. It is called  $f_{subs}$  and defined as the power scattered into substrate divided by the total scattered power. Because of the fact that increasing the optical path length is depending on the multiple scattering events, the fraction of light that lost into the air at each surface scattering event should be small. [29]

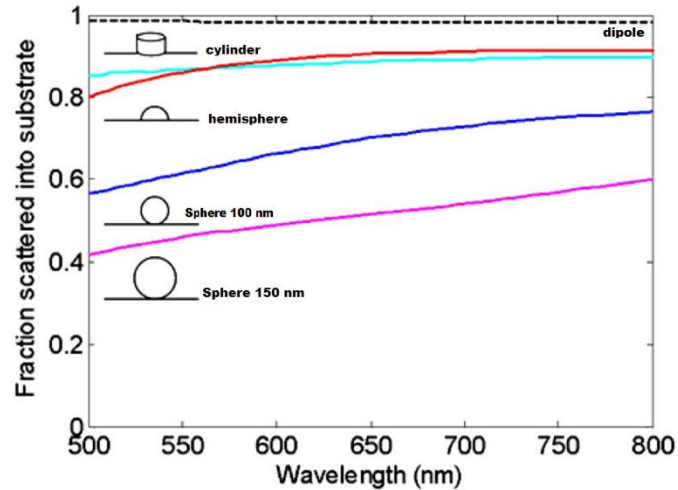


**Figure 3.6** Fraction of light scattered into substrate for Ag nanoparticles on a 10nm thick silicon dioxide under layer on silicon [29]. Purple curve represents the sphere with 150nm diameter blue curve is for 100 nm sphere, red curve represents the hemisphere, and turquoise curve is for cylinder. The dashed line at the top represents the dipole.

As can be seen in the Figure 3.6, for the entire wavelength range the fraction scattered into the substrate for cylinder and hemisphere is much higher than for the sphere. Increase in diameter is important for spheres; when diameter of the sphere increases, the  $f_{subs}$  value significantly decreases. [29]

The high fraction of light scattered into the substrate for cylinder and hemi-spheres is attributed because of the fact that there is a smaller average spacing to the substrate for these geometries, than for spheres. This fact allows the part of the scattered light coupling efficiently that has high-in plane wave vector and is propagating in silicon while evanescent in air. [29]

The angle of propagating of light through the device is another factor that affect the path length enhancement. [29]

The effect of the propagation in Figure 3.7 is described by a factor  $d_{av}$ . This factor is calculated by “the ratio of the path length across a single pass of the device to the device thickness, averaged over the angular distribution of light”. [29]

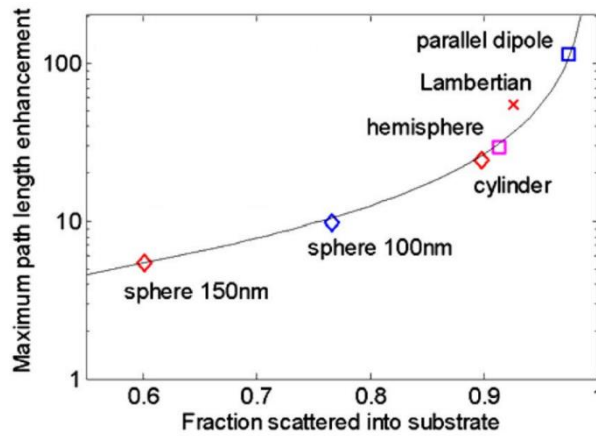


**Figure 3.7** Maximum path length enhancement for the geometries in Figure 2.6 at a wavelength of 800nm [29].

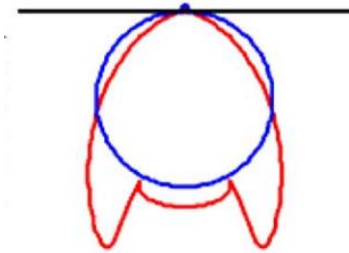


**Figure 3.8** Angular distribution of scattered power for a parallel dielectric dipole that is 10 nm above a silicon surface and Lambertian scatterer [29].

$d_{av}$  is obtained by “performing a weighted integral of  $\frac{1}{\cos \theta}$  over the angular distribution of the scattered power with  $\theta$  as the angle with the normal”. When the distance between the dipole and the substrate increases,  $d_{av}$  decreases. Once  $d_{av}$  and  $f_{subs}$  are known, one can calculated the path length enhancement. [29]

## CHAPTER 4

### EXPERIMENTAL METHODS

#### 4.1 Production of mono-crystalline silicon solar cell:

Fabrication of mono crystalline silicon solar cell consists of six steps; saw damage etching, doping, dry oxidation, deposition of silicon nitride, metallization and laser edge isolation. (Figure 4.1)

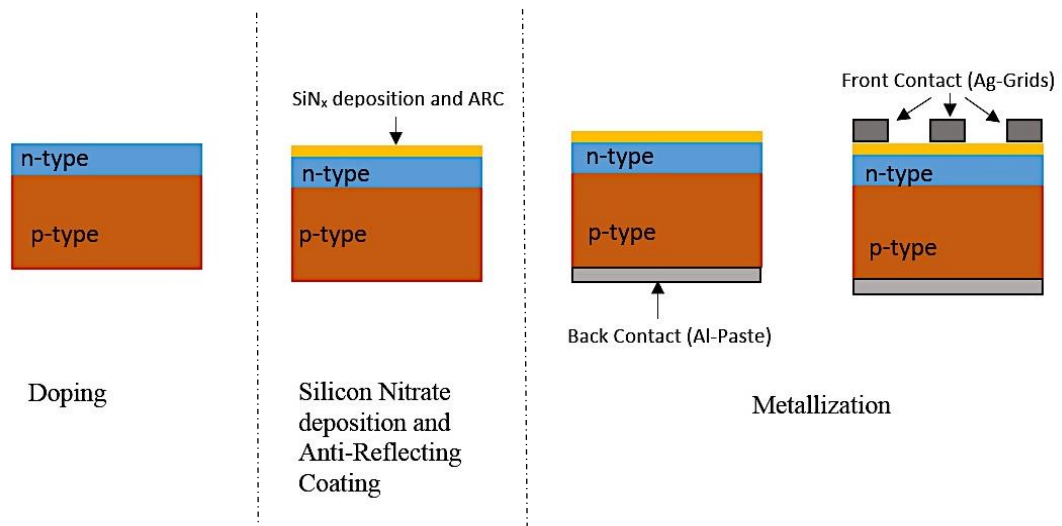


*Figure 4.1 Fabrication process of silicon mono-crystalline solar cell.*

- **Saw Damage Etching:**

The first step of producing mono-crystalline silicon solar cell is saw damage etching. In order to remove any wafer damage caused by wire-sawing, saw damage etching is performed. [30] In this work potassium hydroxide (KOH) is used as etching solution. After saw damage etching, solar cells have either flat or textured surfaces depending on the request. In this study, there were no other processes than saw damage etching.

- **Doping:**

Silicon is a semiconductor material and as in all other semiconductors, silicon does not conduct much electric current in normal conditions. But if silicon heated up to high temperatures or doped with specific material, it starts to conduct electric current.[31]

In order to obtain p-n junction inside silicon, the silicon wafer is doped with boron. This process takes place under low vacuum conditions in a tube furnace with  $\text{POCl}_3$  diffusion. Because of diffusion process, a glass layer is formed. To remove this layer, sample is etched by dilute hydrofluoric acid (HF) dipping and this process ends by standard cleaning procedure. [32]

- **Dry Oxidation:**

The next step is dry oxidation at low temperature to create nearly 10nm thick silicon dioxide ( $\text{SiO}_2$ ) layer to enhance surface passivation.

- **Deposition of Silicon Nitride ( $\text{SiN}_x$ ):**

After oxidation, the front surface of the cell is deposited by silicon nitride ( $\text{SiN}_x$ ). This layer not only acts as an antireflection coating but also improve the quality of surface passivation. The deposition of  $\text{SiN}_x$  is executed in a parallel plate, PECVD system at around  $400^\circ\text{C}$ . [32] The silicon nitride thickness can be detected by the color of the solar cell. The color scale of the nitride thickness is shown at Figure 4.2. [33]

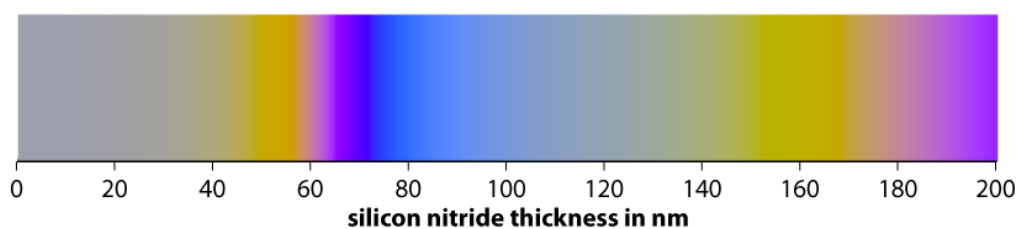


*Figure 4.2: Color scale of nitride thickness on solar cell.*

In this study, three different nitride thicknesses which are 5-10nm, 10-15nm and 18-20nm, will be analyzed. All of the samples are colored in grey.

The reason why three different and thin nitride thicknesses were analyzed is that the radius of the nanoparticles that produced through pol-yol synthesis is around 50-100nm. In order to observe the effects of nanoparticles in terms of plasmonic effects, the silicon nitride thickness should be small not to behave like arc.

- **Metallization:**

The following step is metallization. The metal pattern on the front side is defined as the H patterned silver (Ag) grid and carried out by the industrial screen printing method. The rear side metallization was done by thermal evaporation of aluminum (Al). After metallization processes, the front side grid is firing in an industrial 8-zone firing furnace. [32]

- **Laser edge isolation:**

This whole process is ended up by laser edge isolation to prevent shunt current between front and rear surfaces caused by n-layer deposition.

#### **4.2 Polyol Synthesis of Silver Nanoparticles:**

The dissolution of a protecting agent or stabilizer in a polyol medium is the main part of the general polyol process. Then the required silver precursor is added to this solution. Although the synthesis process of monodisperse silver nanoparticles is well established, little is known about the influence of precursor injection during the polyol synthesis. [34] The polyol process is based on the reduction of an inorganic salt by a polyol at an elevated temperature. A surfactant is used to prevent agglomeration of the colloidal particles.[35]

In this work; ethylene glycol (EG) was used as both solvent and reducing agent, poly(vinylpyrrolidone) (PVP) was used as stabilizing agent and finally silver nitrate ( $\text{AgNO}_3$ ) was used as Ag source.

##### **4.2.1 Procedure:**

All glassware used in the experiment were cleaned with deionized water, acetone, isopropyl alcohol and finally deionized water. In the experiment 10mL of EG solution of PVP was prepared and 500mg NaCl was added to the solution. After that the solution was heated up 80°C with 1000 rpm rate on a hot plate. Meanwhile 200mg  $\text{AgNO}_3$  was added to 10mL of EG solution and then this solution stirred with 1000rpm rate to mix up.

At the end second solution added dropwise into PVP solution by injection pump at a rate of 5mL/h. (Figure 4.3)



*Figure 4.3 Photo of silver nanoparticle synthesis setup.*

#### **4.2.2 Purification part:**

For separation the polymer from the silver nanoparticles (AgNPs), the solution centrifuged two times at seven thousands rpm rate for twenty minutes.

One third of the centrifuge tubes were filled with AgNPs solution and diluted with acetone. ((CH<sub>3</sub>)<sub>2</sub>CO) (530gr each tube) And centrifuge started.

After twenty minutes first centrifuge was over and the solution on the top of the centrifuge tubes were emptied to the sink. To make sure there are only AGNPs were stayed in the tubes, we again centrifuged the remaining product.

The remaining product were diluted with acetone and centrifuged again.

Twenty minutes later, centrifuge was over. The solutions on the top were emptied again. This time remaining AgNPs were dispersed with ethanol (C<sub>2</sub>H<sub>5</sub>OH) for further characteristics. (Figure 4.4)



**Figure 4.4** Photos of 1, 2 and 3; Synthesized AgNPs solutions without purification and 4; AgNPs in ethanol.

### 4.3 Spray Coating Technique

The spray coating technique is mainly used for graphic arts, industrial coatings and painting. It generally lets us to deposit large areas which have different morphologies. Also, by spray coating we have a chance to access a broad spectrum of fluids with different rheologies and to tune the system for depositing any kind of solution [36] (Figure 4.5).

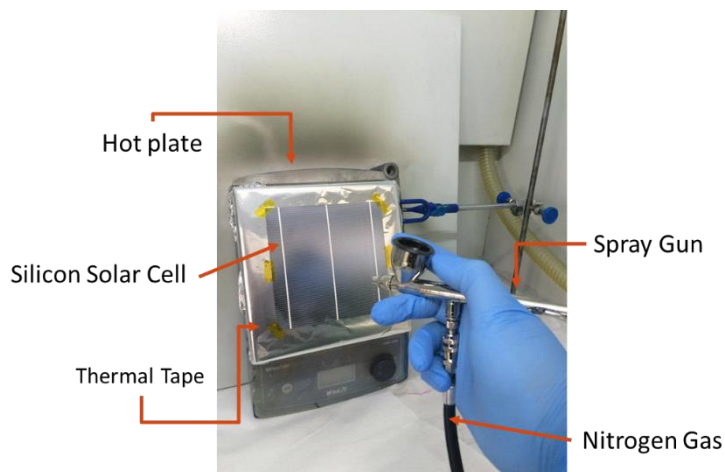


**Figure 4.5** Spray Coating Technique

Spray coating is a multistep method that includes atomization of liquid solution or mixture, droplet flight and evaporation, droplet impact on the substrate, droplet spreading, receding, recoiling, drying, solute adhesion and bonding to itself and the substrate. [36]

This technique is performed at atmospheric pressure and among other solution processes, spray coating is thought to be the one of the cost-effective coating methods. [36]

Although handheld airbrushes are used for this technique, it is still seen as a promising and scalable deposition technique. [36]

## 4.4 Optical Characterization

### 4.4.1 Reflection Set-Up:

The reflectivity properties of the samples were measured as shown in the Figure 4.6. The elements of the set-up are following; integrating sphere, lock-in amplifier, chopper and controller, calibrated silicon detector, halogen lamp, monochromator, focusing lens and computer.

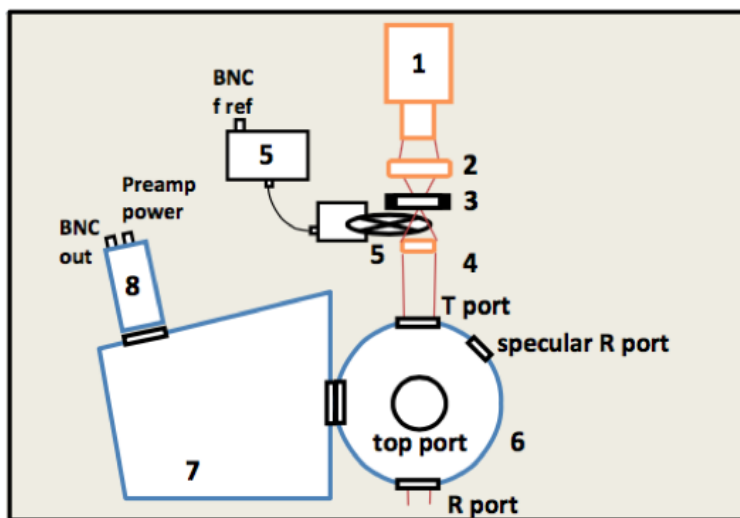


*Figure 4.6 Schematics of Reflection Measurement Set-up [37].*

In this study, samples were coated with silver nanoparticles so there were both specular and diffuse reflection as shown in Figure 4.7.

In order to measure specular and diffuse reflectivity, an integrating sphere (70679NS) was used.

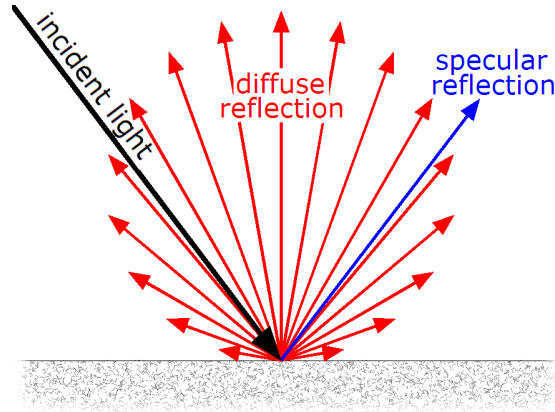


**Figure 4.7** Types of Reflection.

Before starting measurement of the samples, a calibration disk ( $\text{BaSO}_4$ ) placed at the integrating sphere reflection port to measure the hundred percent reflection as a reference data. The real reflectance of our  $\text{BaSO}_4$  disk is below 100%. A reflectance dataset for  $\text{BaSO}_4$  ( $R_{\text{BaSO}_4}$ ) is used to account for this when calculating the sample reflectance. [38] Second step was leaving empty reflection and transmission ports of the integrating sphere to measure “dark”. Dark means zero reflection. It was done to obtain more accurate data. After measuring reference, dark and sample, following calculation was done to get specular reflection data;

$$R_{total} = \frac{R - Dark}{\frac{R_{ref}}{R_{\text{BaSO}_4}} - Dark} \quad (4.1)$$

Diffuse reflection measurement was slightly different from the specular reflection measurement. While measuring the diffuse reflection, one port of the integrating sphere left open and protected from light coming from halogen lamp. Reference and dark measurements were again done. Following calculation gives the diffuse reflection data:

$$R_{diffuse} = \frac{R^* - Dark^*}{\frac{R_{ref}^*}{R_{\text{BaSO}_4}} - Dark^*} \quad (4.2)$$

\* represents the data which was taken while one port of the integrating sphere left open

The scattering of light that caused cloudiness of a product is called haze. [39] In this study diffuse reflection of the samples measured to determine the percentage of the haze and it is calculated by following equation:

$$Haze(\%) = \frac{R_{total}}{R_{diffuse}} \times 100 \quad (4.3)$$

#### 4.5 Electrical Characterization:

##### 4.5.1 I-V Measurements:

Cell efficiency, fill factor, open circuit voltage and short circuit current of the solar cells are measured by AM 1.5G calibrated QUICK SUN-120CA-XL Solar Simulator, provided by GÜNAM laboratory. Simulator software analyses the I-V measurement and determines the above mentioned features.

Standard area of the solar cell in this study is 0.0169 m<sup>2</sup>. All of the calculations made by simulator are based on this value. Sample is connected by two probes in front (fingers) and back (copper plate) contact of solar cell to the current-voltage source and the computer software controlling solar simulator and source meter. (Keithley) (Figure 4.8)

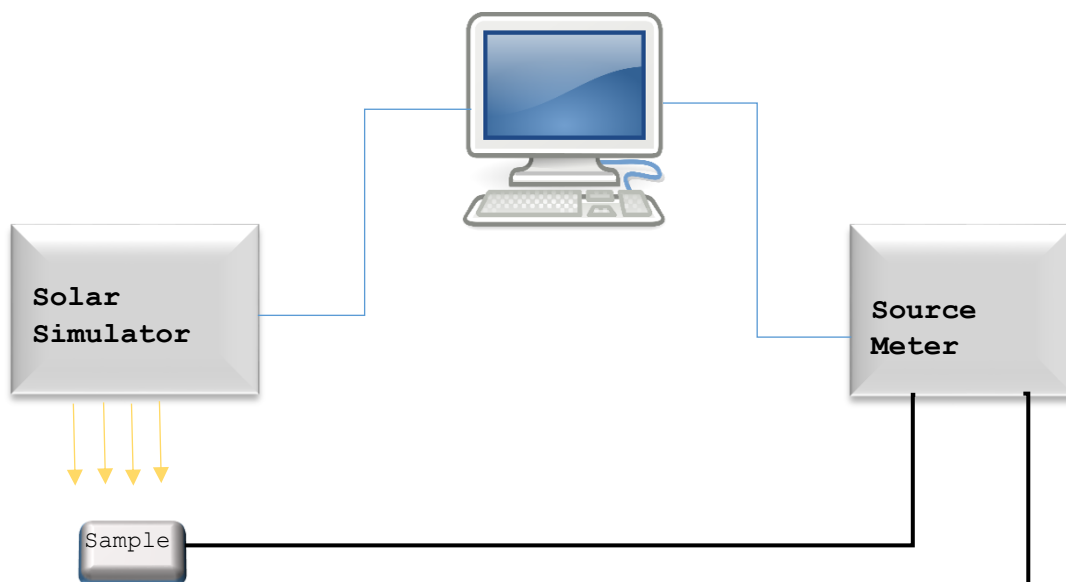


*Figure 4.8 Schematic drawing of I-V Measurement Set-up.*

### 4.5.2 Quantum Efficiency Set-up:

Quantum efficiency measurements were conducted with set-up shown in Figure 4.9;

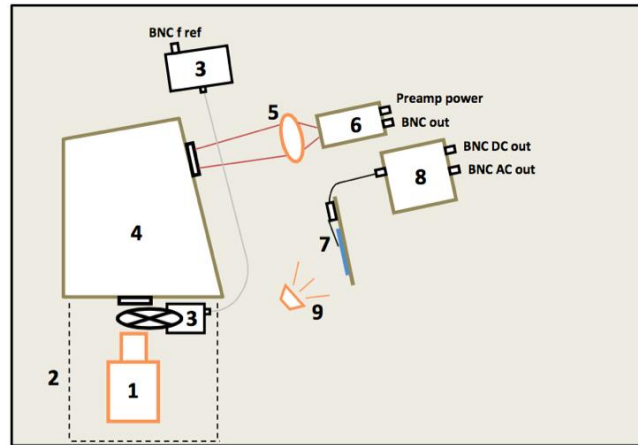


**Figure 4.9** Schematics of Quantum Efficiency Set-up [40].

Set-up consisted of 100 W halogen lamp and radiometric power supply (68831), black box, chopper wheel and controller, monochromator (74100), condensed lens (focal length 8 cm), photodetector (70356) and Merlin power supply, solar cell, current to voltage amplifier (70710) and LED for light bias. (Figure 4.9)

For a given wavelength, the ratio of the number of electrons generated by a solar cell to the number of photons that impinge on the top surface is called external quantum efficiency. [40] This set up measures the quality of the solar cell in terms of converting the light of that particular wavelength.

The fundamental concept of EQE measurement is the comparison of two photocurrent measurements of which detector with known responsivity and measured cell. These measurements are done under the same illumination conditions. [40]

$$EQE(\lambda) = \frac{\text{photon count}}{\text{electron count}} \quad (4.4)$$

By the help of reflection measurement, the internal quantum efficiency of the solar cells, that is the ratio of number of electrons generated by solar cells to the number of absorbed photons by considering losses caused by reflection, can be calculated. [40]

$$IQE(\lambda) = \frac{EQE(\lambda)}{1-R(\lambda)} \quad (4.5)$$

## **4.6 Image Analysis Method:**

In order to determine the surface coverage of devices and homogeneity of spray coating, samples were imaged with Zeiss EVO HD 15 Scanning Electron Microscopy (SEM) at GÜNAM Facility. By SEM images, the formation of silver nanoparticles be observed in terms of shape and size. This observation is important for deciding the plasmonic principle behind measurements and results.

Later on taken images were analyzed by image analyzing software program named Gwyddion. This analysis provides to determine the qualitative and quantitative characteristics of images as told before.

To give an idea of how Gwyddion software works, an analysis of a solar cell is given as an example below.

The exemplary solar cell has the following characteristics; 10-15 nm silicon nitride thickness, 20 times spray passes. This sample was taken from the center of the solar cell. (In later analyzes this sample will be named 220A.)

### **4.6.1 Example Analysis:**

Before starting the analyzing procedure, the pixel size of the software and magnification of the SEM image were optimized. All magnifications are set to 20 K for correct analysis.

The first step of the analyzing procedure is removing the polynomial background. This process is needed because the surfaces of solar cells are textured-like due to saw damage etching. At the end of this process, the surfaces of the devices may treat to function as if they are flat. So that the sizes and distributions of the particles are more accurately determined.

Second step is creating a mask to mark the grains by threshold. This step provides to detect silver nanoparticles on the surface, therefore the number of them. Then, the surface coverage rate (%) can be calculated through software.

After completed all analyzing steps for aforementioned sample, the surface coverage of it was determined as 3.84%.

Detailed analyzing steps are given in Figure 4.10;

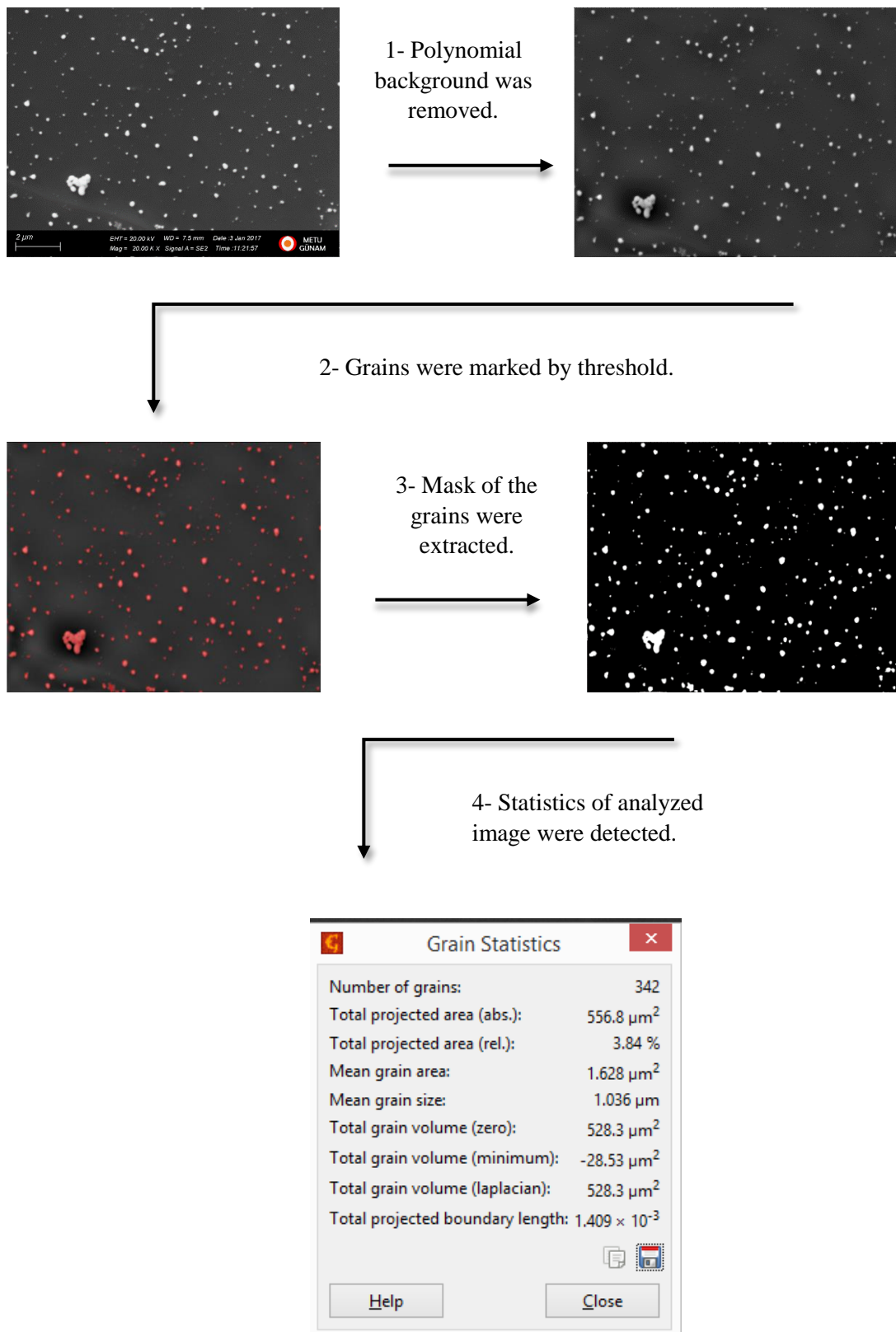


**Figure 4.10** Schematic representation of image analyzing procedure.

The analysis of all samples in terms of SEM imaging, specular reflection, diffuse reflection and EQE measurements and current-voltage (I-V) curves are given at results and discussion part in detail.

## CHAPTER 5

### RESULTS AND DISCUSSION

In this study, by using aforementioned experimental strategies, the effects of metal nanoparticles for improving the cell efficiency is examined for the solar cells have three different nitride thicknesses; ~5-10 nm, ~10-15 nm and ~18- 20 nm. These three different thicknesses are defined as three sets, and the sets are referred to as SET 1 SET 2 and SET 3, respectively, with increasing nitride thickness.

For investigating the silver nanoparticles' plasmonic effects, these three sets will be examined individually in terms of change in efficiency, amount of surface coverage, change in current-voltage (I-V) curve, reflection, haze and quantum efficiency measurements.

Before deciding the number of spray coating passes for solar cells, there was a trial on silicon wafers. The silver nanoparticles (Ag NPs) synthesized by the polyol technique were sprayed on silicon wafers at a distance of 6-8 cm with a pressure flow of 1.5 bar. (Same conditions were valid for this thesis study.) After spray coating, the surface coverage rates were determined with Gwyddion software using SEM images.

As can be seen in the graph below (Figure 5.1), the surface coverage rates determined for 20 to 50 passes are between 7.94 and 20.51%. These outcomes show that by decreasing the number of spray passes, desired surface coverage rate can be met.

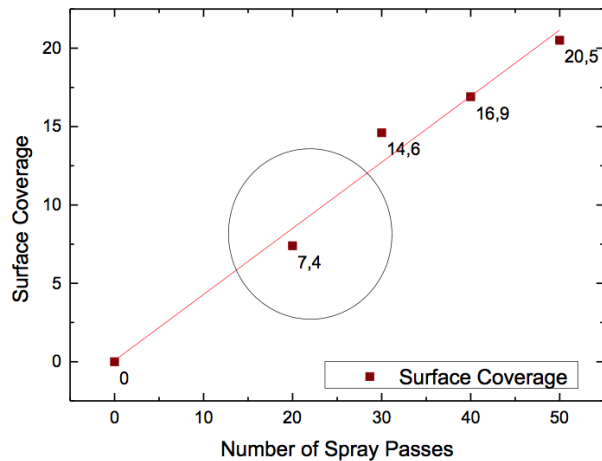


**Figure 5.1** Surface Coverage vs. Number of spray passes graph of aforementioned study with flat silicon wafers. The linear fit suggests an approximately 4% added surface coverage for each spray pass.

As mentioned in the introduction part, the aim of this work was to fall below about 30% of surface coverage and provide it around 10%. So it was decided that the number of passes would be 10-15-20-25 and 30 in order to catch the 10% value for the solar cells

In this study, in order to identify the difference in efficiency of the solar cells individually, samples were measured with solar simulator before and after spray coating. With this measurement not only the change in efficiency but also variation in current-voltage (I-V) curves were obtained.

The solar cells were measured twice in a solar simulator to determine whether the particles were broken down over time. As a result of these measurements it has been found that the increase in efficiency (%) did not show any significant change. So, the particles did not deteriorate over time. This information is shared in a column of the sets' efficiency tables.

In solar simulator solar cells were measured in full size (13cm-13cm). After solar simulator measurement, the dimensions of the solar cells were reduced to 4 cm to 3cm by laser as shown in Figure 5.2. This reduction is necessary for reflection, diffuse reflection, external quantum efficiency measurements and SEM analysis.



**Figure 5.2** Photo of Laser Cut Set-Up.

The laser parameters are as follows: Power; 100%, Frequency; 45 kHz, Number of passes; 23.

Solar cells were cut according to following sketch (Figure 5.3) for detailed examination;

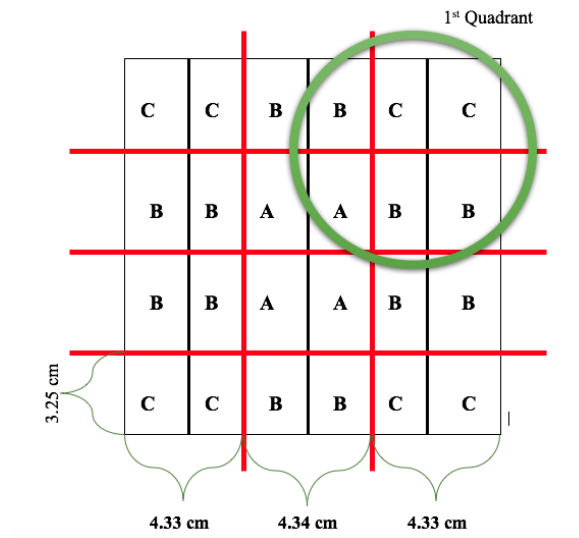


**Figure 5.3** Sketch of laser cut process

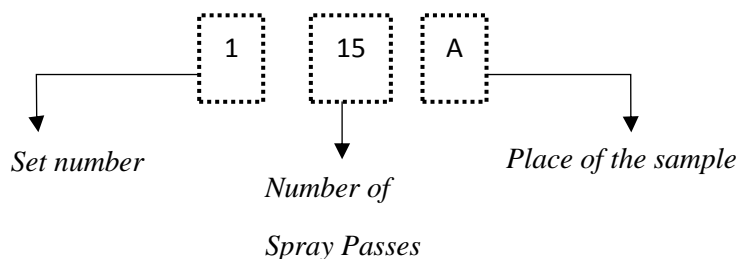
- Red lines refer to bus bar of the solar cells
- Black lines refer to cutting lines

All remaining measurements; specular and diffuse reflection, quantum efficiency and SEM imaging were done according to this sketch as said earlier.

Measurements were completed by taking two different samples from regions marked A, B and C. That provides to examine nearly all surface of the solar cell. This detailed examination was made for the possibility that all parts of the solar cells were not evenly covered during spray coating.

The samples were named according to their nitride thicknesses, number of passes and places.

Example: A sample has 5-10nm nitride thickness (SET 1), 15 times passes and at A part of the cell is named as; “115A”



After laser cutting process, the optical characterization of the plasmonic interfaces and photovoltaic properties of the solar cells were analyzed.

Optical Characterization:

- Specular and diffuse reflection of the samples were measured with integrating sphere. And haze of the solar cells was calculated through these data.

Electrical Characterization and Photovoltaic Properties:

- The first measurement of this part is quantum efficiency.
- After that solar simulator was used to identify the photovoltaic characteristics like fill factor ( $FF$ ), open circuit voltage ( $V_{oc}$ ), short circuit current ( $I_{sc}$ ) and efficiencies ( $\eta$ ) of devices.

SEM Imaging:

- All parts of the SETs (A, B and C) were analyzed with SEM.
- After SEM analysis, surface coverage of each sample were calculated by the help of Gwyddion software program.

The characterization results are given separately for each measurement, covering each set.

## 5.1 Reflection Measurements Results:

It is necessary to talk about an exceptional situation before deeper analyzes and interpretations are made. A different situation has been observed for one device at SET 1, which was coated 25 times, as evidenced by the decrease in the efficiency value. This situation is explained in detail in the brief discussion section after the conclusion part. In the remaining analyzes, this sample was drawn out in order not to break the set and necessary graphics were drawn and comments were made in this direction.

As mentioned earlier, solar cells were cut and three different samples taken from different parts of the cell (A, B and C at Figure 5.3) were measured for deeper analysis. The specular and diffuse reflection measurements of the samples were made for parts A, B and C, respectively.

For each location, two different samples were chosen and measured for the probability of inhomogeneous coating, and also the certainty of the measurements.

In the graphs there were two curves; one solid and one dotted. The dotted curves represent the results of the second sample taken from the same region, labeled as “2”. (Like “115A” and “115A 2”)

### 5.1.1 Reflection graphs of SET 1 (5-10 nm Silicon Nitride):

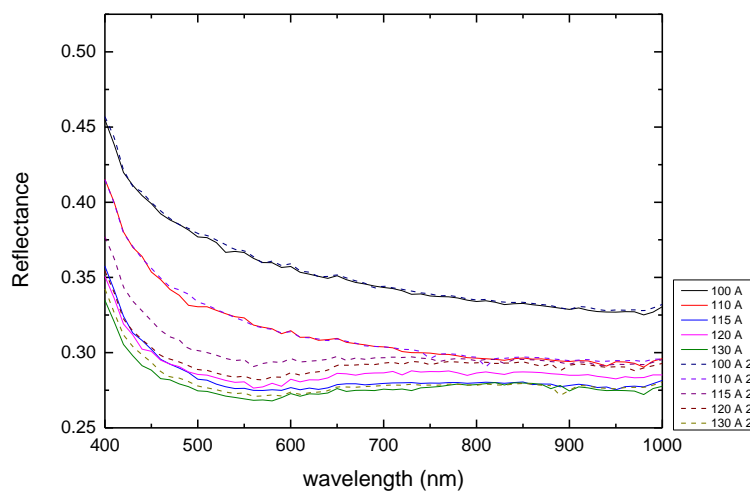


*Figure 5.4 Reflectance Graph of A for SET 1.*

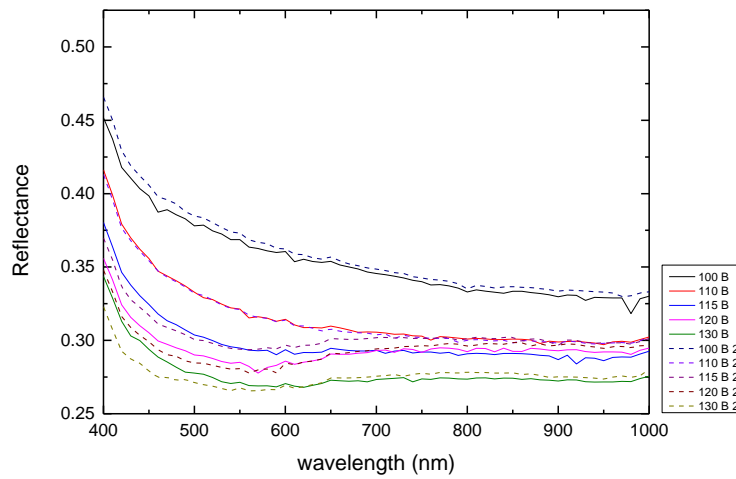


**Figure 5.5** Reflectance Graph of B for SET 1.

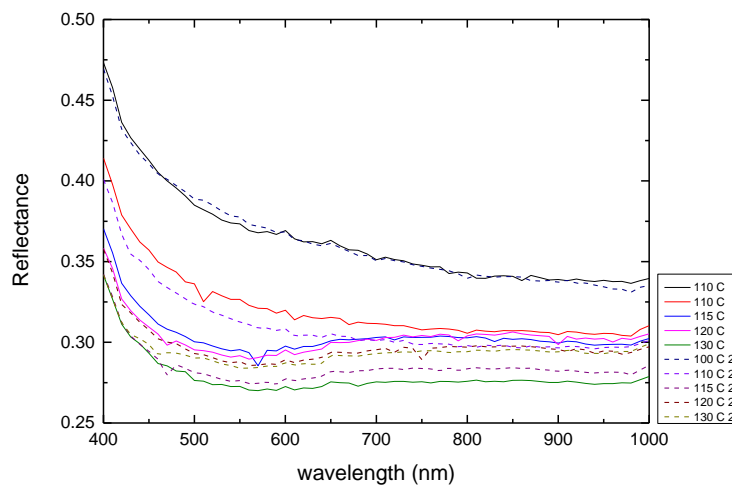


**Figure 5.6** Reflectance Graph of C for SET 1.

When the reflectance graphs are examined, it is clearly seen that number of spray passes and reflectance of the samples are inversely proportional to each other, as expected. Nanoparticles that sprayed onto solar cells act like anti-reflection coating and decrease the reflection of the solar cells. The lowest reflectance value belongs to sample with the highest number of spray passes while the highest reflectance value belongs to the reference sample (uncoated).

### 5.1.2 Reflection Graphs of SET 2 (10-15nm Silicon Nitride):

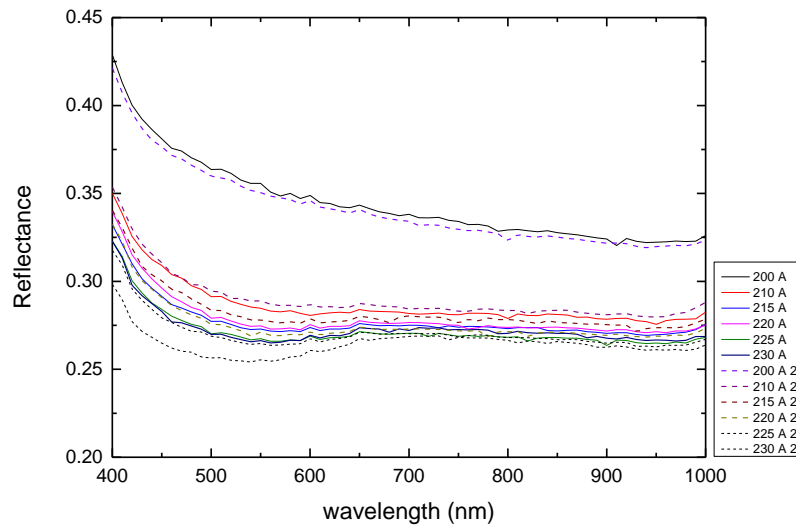


*Figure 5.7 Reflectance Graph of A for SET 2.*

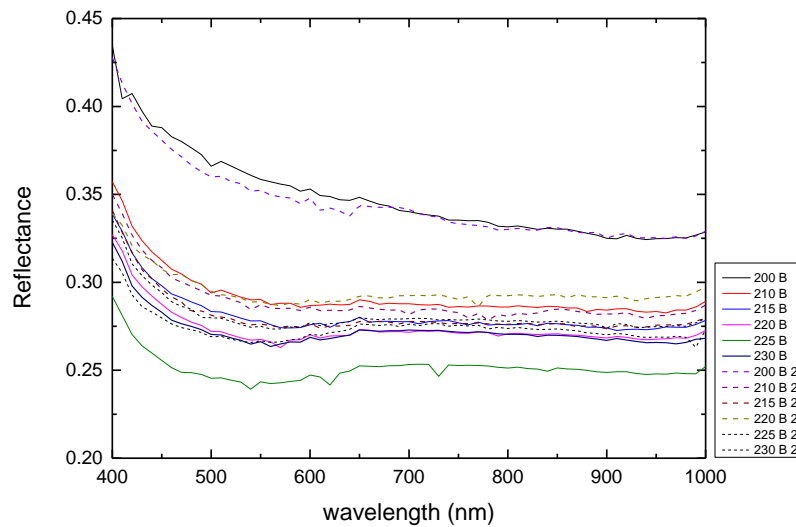


*Figure 5.8 Reflectance Graph of B for SET 2.*

When Figure 5.8 is inspected, difference between green solid line and green dotted line is drew attention. (230B and 230B 2) This difference is a negative outcome of spray coating, inhomogeneous coating. Two different samples were measured from the same position already considering this possibility.

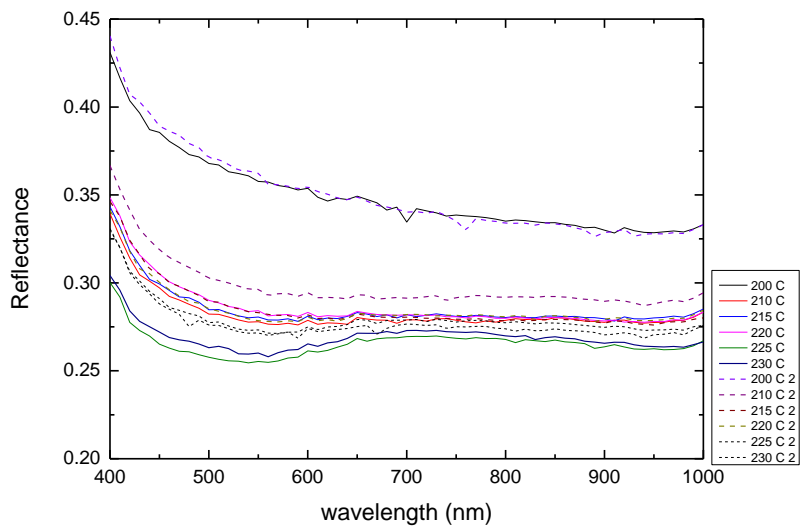


**Figure 5.9** Reflectance Graph of C for SET 2.

Comments about the effects of nanoparticles on reflection values that for SET 1 are also valid for SET 2. But there is a different situation for the second set; the reflectance values of the sample coated 25 times are less than the sample coated 30 times. This data indicates that the particles may have been overlapped on the sample coated 30 times. So that the surface coverage rate of the sample coated 25 times may be higher. Hence, the reflection value is lower for that sample.

**5.1.3 Reflection Graphs of SET 3 (18-20 nm Silicon Nitride):**

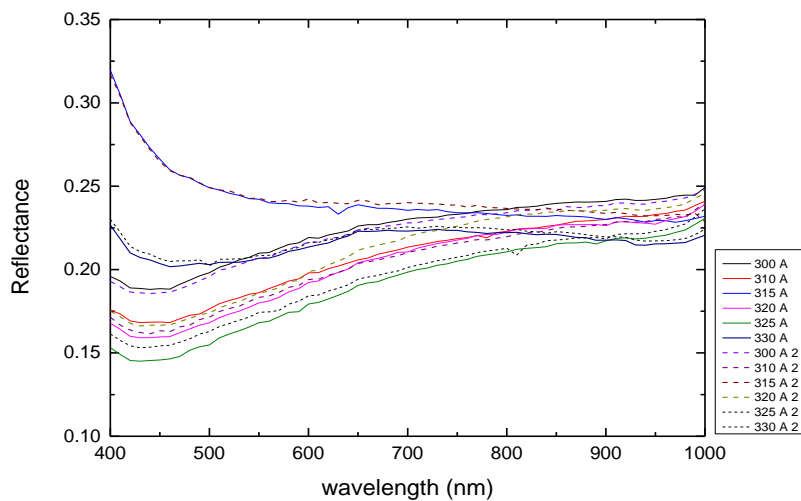


**Figure 5.10** Reflectance Graph of A for SET 3.

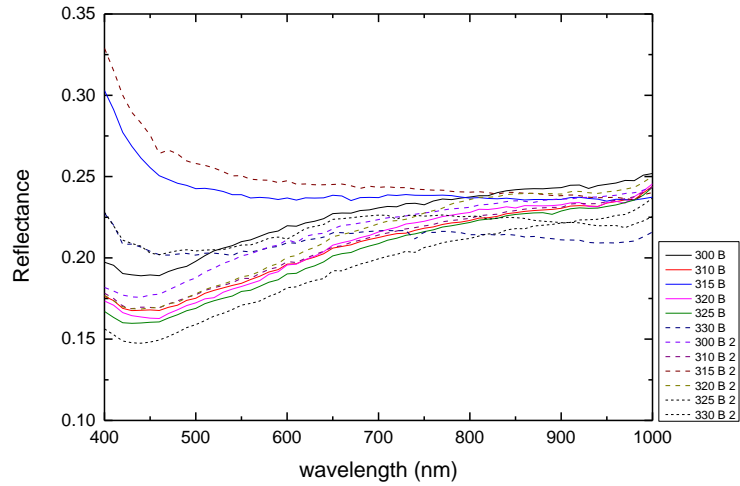


**Figure 5.11** Reflectance Graph of B for SET 3.

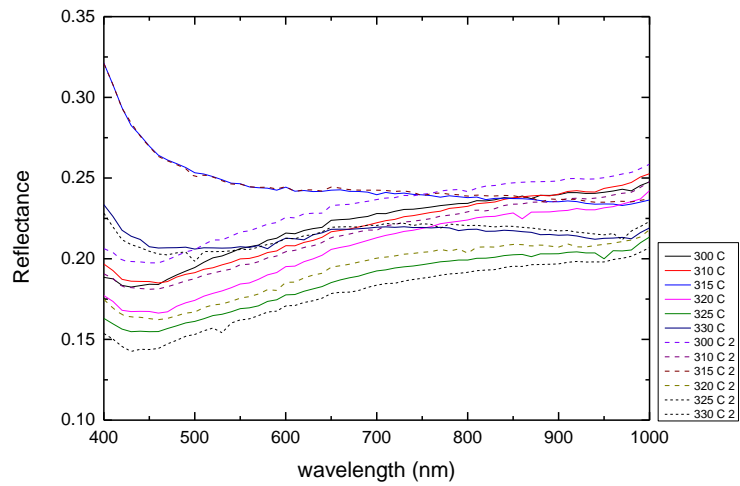


**Figure 5.12** Reflectance Graph of C for SET 3.

When the reflectance graphs of SET 3 are investigated, the difference of the curves than SET 1 and SET 2 can be clearly seen. The difference in the curves is caused by the difference in the structure of the surfaces of the solar cells in this set. When the SEM images were analyzed, the depth of the squares that caused by saw damage etching is the highest for SET 3 among all sets. Hence, this highest depths causing the anomaly in reflectance graphs. But, in terms of nanoparticles effects through spray coating on reflection values, above comments are again valid for SET 3.

## 5.2 Diffuse Reflection Measurements Results:

The results of previous trial on silicon wafers and this study are similar in terms of specular reflection measurement as shown above. On the other hand, in diffuse reflection measurement, the results of silicon wafer trials and the results of this study are contradictory. Trial results indicate that the number of spray passes is directly proportional to diffuse reflectance values. But in this study, the change in diffuse reflectance values are inversely proportional to the number of spray passes

The major difference between the previous trial and this study is the characteristics of the surfaces of measuring samples. In trial, the flat silicon wafers were measured while in this study “textured-like” surfaces were measured. “Textured-like” surfaces were formed due to saw damage etching as said before. As a result, diffuse reflection values were decreasing as the number of spray passes increasing.

Following diffuse reflectance graphs support that argument for all three sets.

### 5.2.1 Diffuse Reflection Graphs of SET 1 (5-10 nm Silicon Nitride):

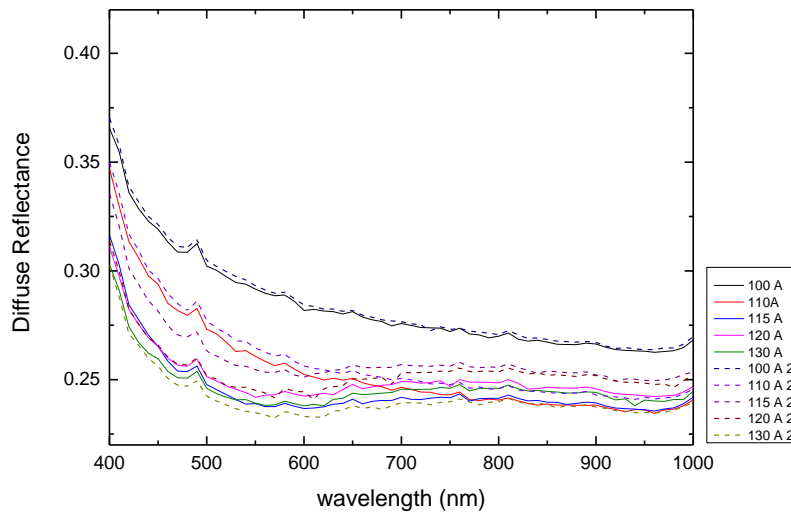


**Figure 5.13** Diffuse Reflectance Graph of A for SET 1.

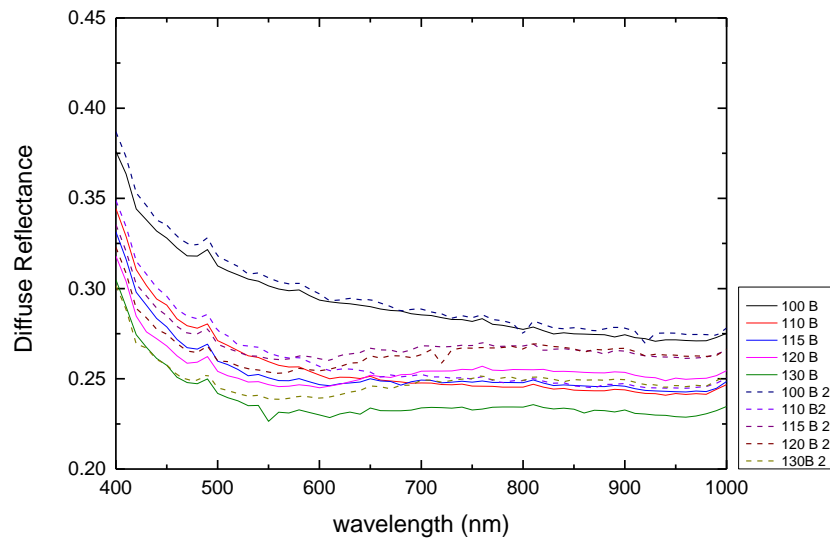


**Figure 5.14** Diffuse Reflectance Graph of B for SET 1.

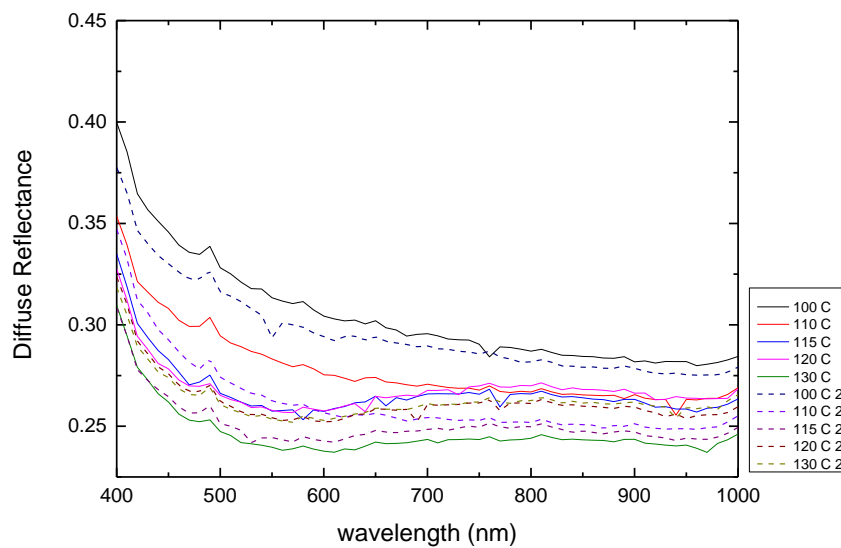


**Figure 5.15** Diffuse Reflectance Graph of C for SET 1.

When the diffuse reflectance graphs of SET 1 examined, it is seen that above argument is supported. The lowest diffuse reflectance value belongs to the sample that coated the highest. (30 times passed, green curves) On the other hand, the reference sample (uncoated) has the highest diffuse reflectance value; this means that spray coating has a negative effect in terms of diffuse reflectance values.

**5.2.2 Diffuse Reflection Graphs of SET 2 (10-15 nm Silicon Nitride):**

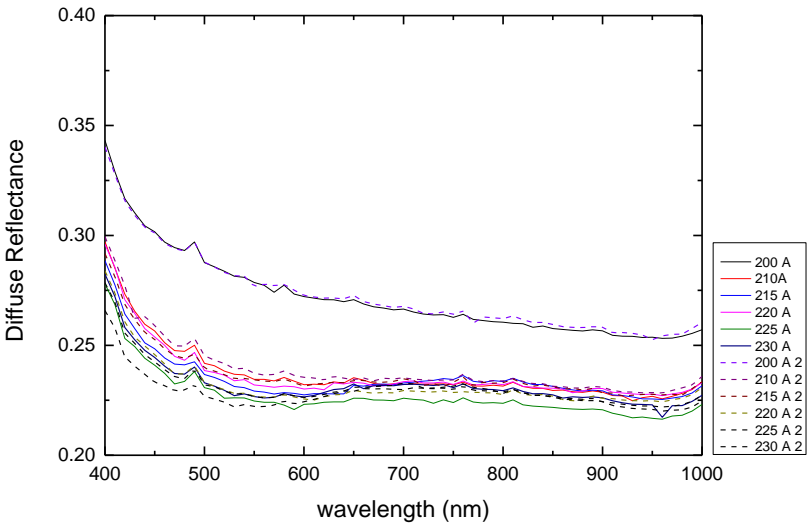


*Figure 5.16 Diffuse Reflectance Graph of A for SET 2.*

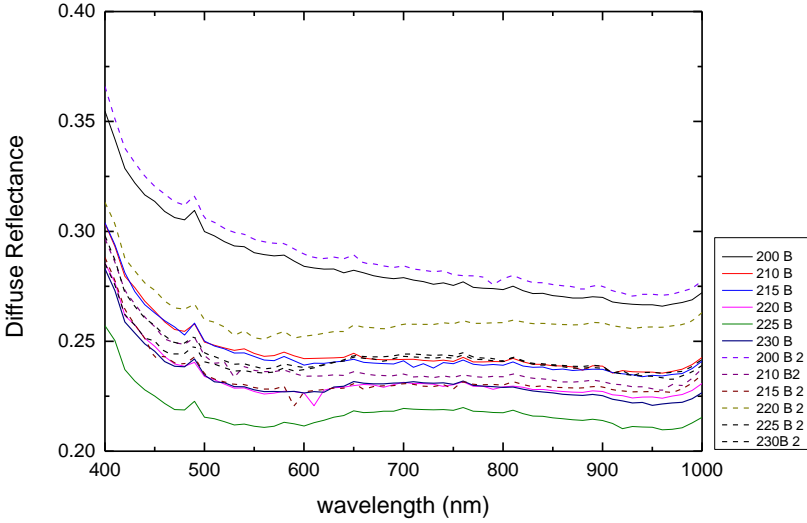


*Figure 5.17 Diffuse Reflectance Graph of B for SET 2.*

When Figure 5.17 is examined, the difference in green solid line and green dotted line can easily be detected. Both of these curves belongs to the sample that coated 30 times. This type of difference, which is a negative side of spray coating, caused by inhomogeneous coating of samples in same region.

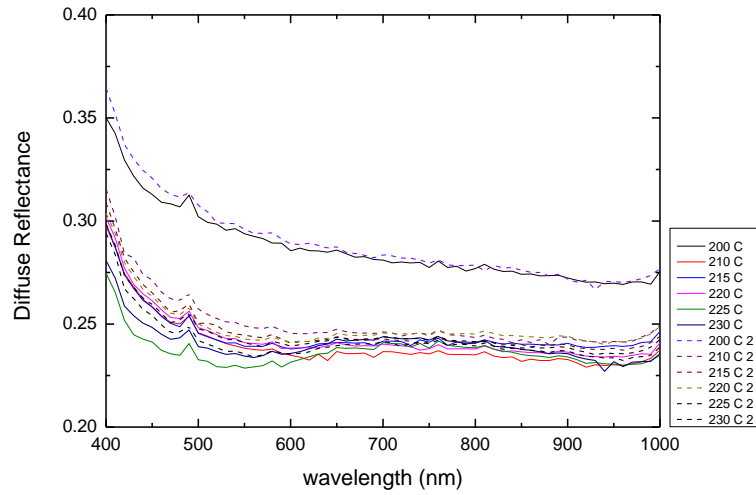


**Figure 5.18** Diffuse Reflectance Graph of C for SET 2.

Previous comments in terms of the relation between the diffuse reflectance values and the number of passes that for SET 1 is valid for this set as well. The only difference between. As the number of spray passes increase, the amount of diffuse reflection decreases for all parts of the samples. (A, B and C)

**5.2.3 Diffuse Reflection Graphs of SET 3 (18-20 nm Silicon Nitride):**

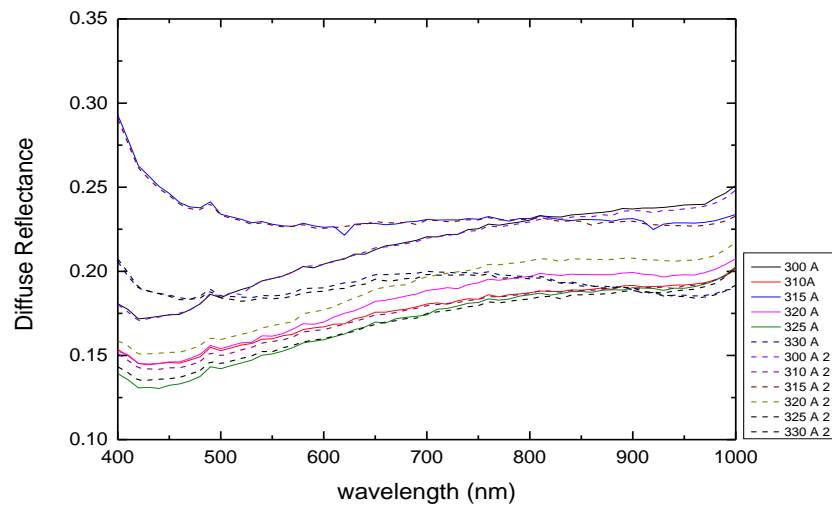


**Figure 5.19** Diffuse Reflectance Graph of A for SET 3.

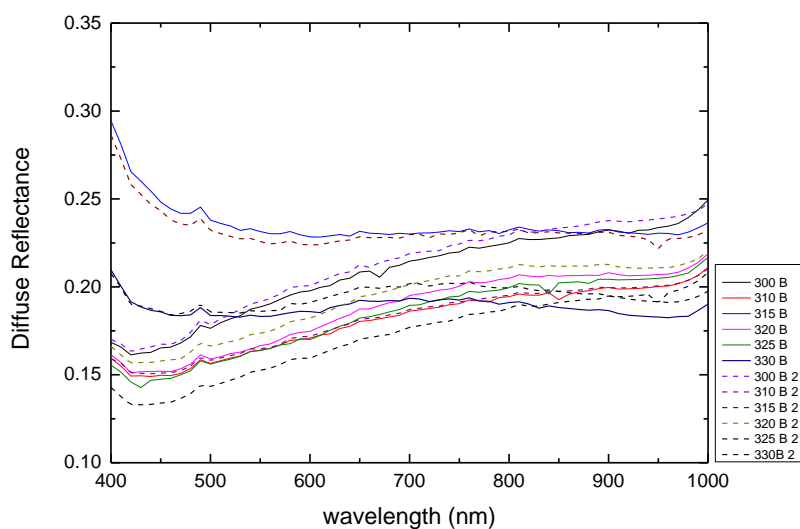


**Figure 5.20** Diffuse Reflectance Graph of B for SET 3.

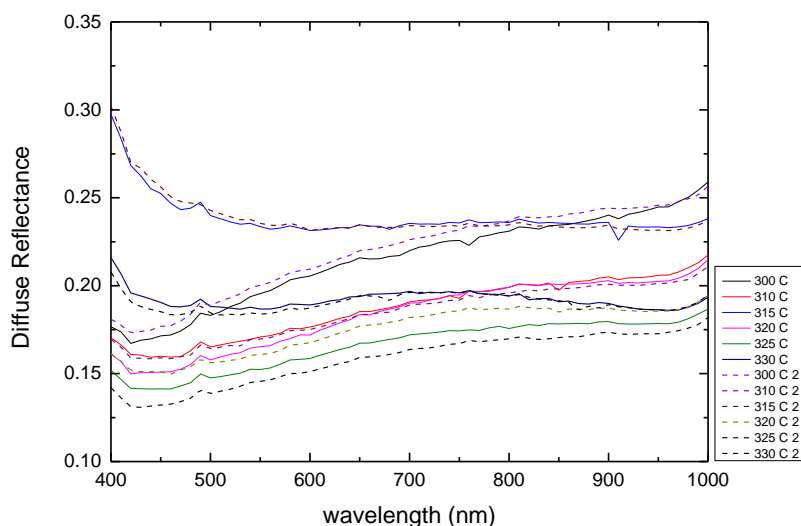


**Figure 5.21** Diffuse Reflectance Graph of C for SET 3.

The same anomaly about curves in reflection graphs of SET 3 again occurred here. The reason also is the same, surface defects. But in terms of the effects of the nanoparticles on the diffuse reflection range, the effect is same with SET 1 and SET 2. There is an inverse proportionality between number of spray passes and diffuse reflectance values. It has been proven through these measurements that the spray coating disperses the particles homogeneously.

Haze of the devices were calculated by using specular and diffuse reflection values, and the details of calculations were told at previous part. The haze graphs on the other hand were not drawn individually, but given in box charts at the end of this section for better comparison.

### 5.3 SEM Imaging Analysis:

In order to determine the surface coverage rates of the devices, the scanning electron microscope images were used with Gwyddion software. The description of the analysis is given at previous part.

For all three sets, two samples that are taken from A, B and C parts of the solar cells were analyzed and total surface coverage rate of the solar cells were calculated through averaging the six individual samples' surface coverage rates.

In order to prevent complexity, only for the A parts of the solar cells' SEM images were shared for all three sets. All of them were taken under 20K magnification.

#### 5.3.1 SEM Images for SET 1:

The square-like shapes are the outcomes of saw damage etching as referred earlier. The shining dots are the tiny pyramids.

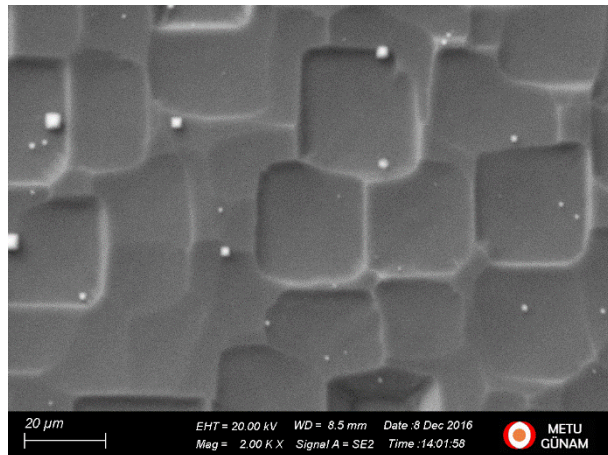


*Figure 5.22 SEM image of the reference (uncoated) device of SET 1 named 100A.*

The depth of the squares and the pyramids are found with SEM image taken with 75° tilt. (Figure 5.23)

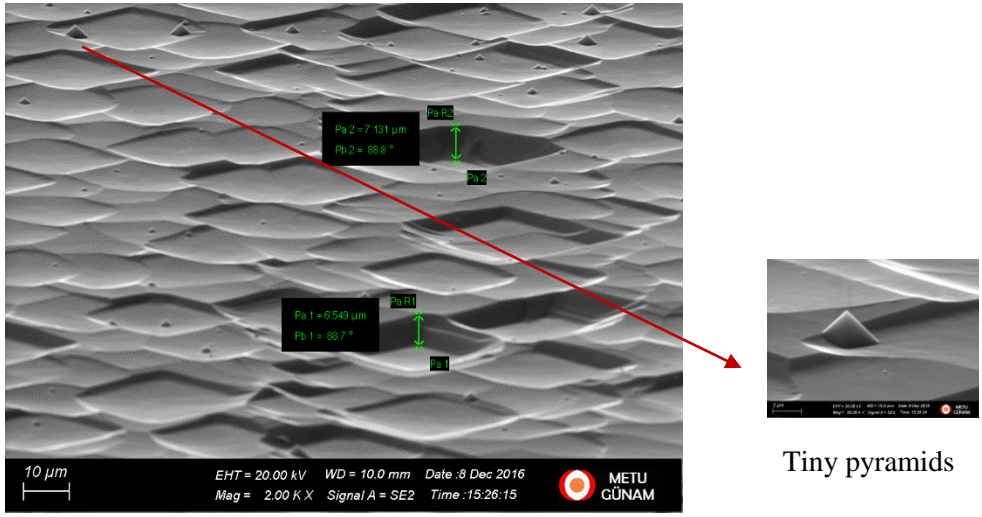
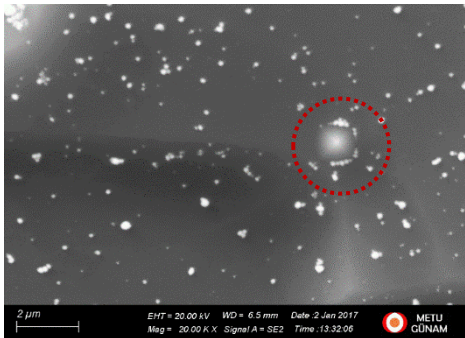


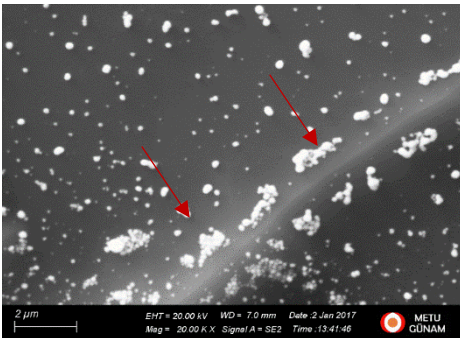
**Figure 5.23** SEM image of the reference (uncoated) device (100A) with 75° tilt.

The approximate depth of the squares is around 6.54 – 7.13 μm.

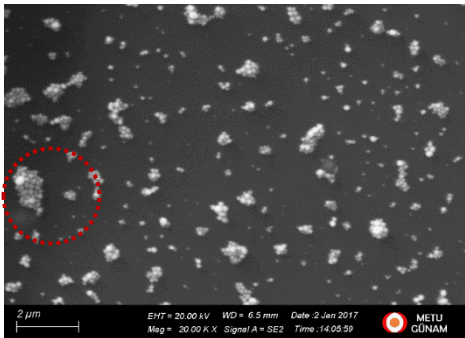
SEM images of coated devices in ascending order in terms of number of spray passes;



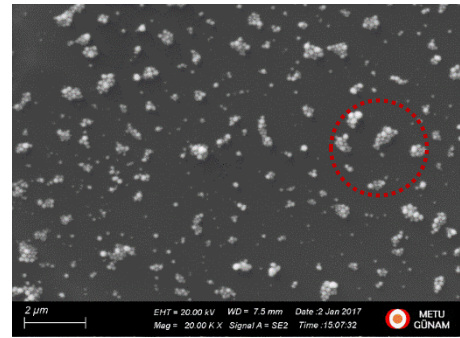
**110 A**



**115 A**



**120 A**



**130 A**

**Figure 5.24** SEM images of SET 1 (A parts, 20K Magnification).

When the SEM Image of 110A is examined, small pyramid and nanoparticles collected on the sides of this pyramid can be seen. Besides, in the SEM Image of 115A nanoparticles gathered near the edges of the square structures are easily detected. Particles tend to cumulate near these edges and this affect the efficiency in a negative way. Increase in number of spray passes caused agglomeration of particles.

In SEM Images of 120A and 130A the agglomerated particles can be seen. There is not an order in agglomeration but they look like little clouds. (Marked zones)

### 5.3.2 SEM Images for SET 2:

The SEM images were taken under 2.00K magnification for general view of the solar cells' surfaces. If the SEM image of 100A (Figure 5.23) and 200A (Figure 5.25) are compared, the difference of the size and the order of the square-like defects on the surface be easily detected. The size of the squares in 200A is much bigger than 100A.



*Figure 5.25 SEM image of the reference (uncoated) device of SET 2 named 200A.*

This information plays an important role for this thesis because it has been observed that sets with different nitride thicknesses differ from each other in terms of surface structure. It has been determined that comparing these sets with each other will not provide meaningful information.

When the sets are examined by-one-by, the structural differences in the surface are again observed. (As understood from the SEM images of the coated samples Figure 5.24) So that each sample was measured before and after coating and was assessed within itself as previously stated.

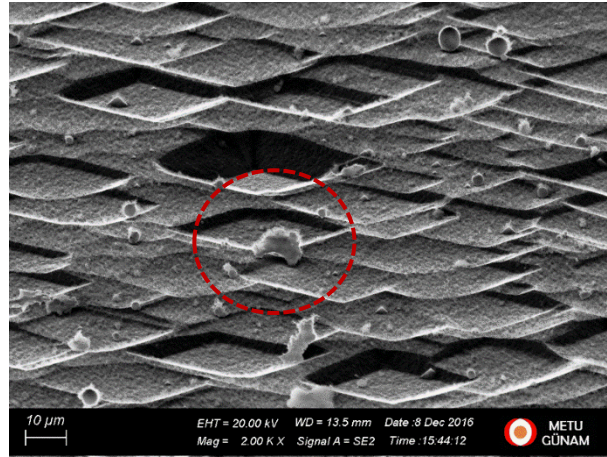


*Figure 5.26 SEM image of the reference (uncoated) device (200A) with 75° tilt.*

When the marked zone on Figure 5.26 is investigated, the particle-like defects can be seen. These defects are maybe caused by saw damage etching method or silicon nitride coating step. At first they seemed like dirt, but further analysis refutes this possibility.

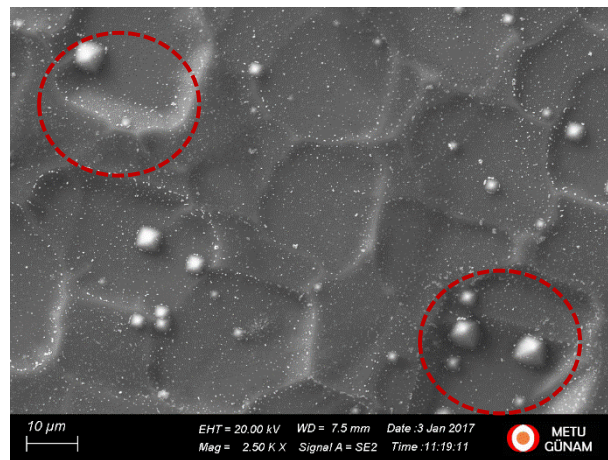
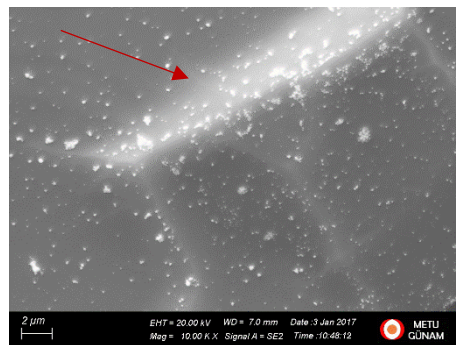


*Figure 5.27 SEM image of the sample named 220A*

The marked zones on Figure 5.27 points out the small pyramids caused by saw damage etching process.

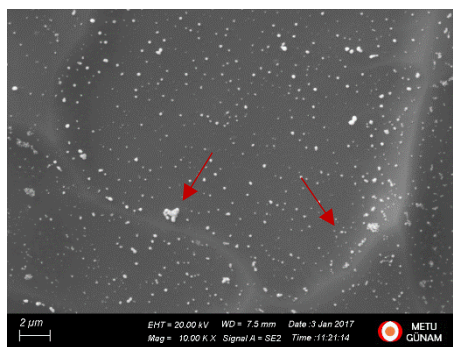
SEM images of coated devices in ascending order in terms of number of spray passes;



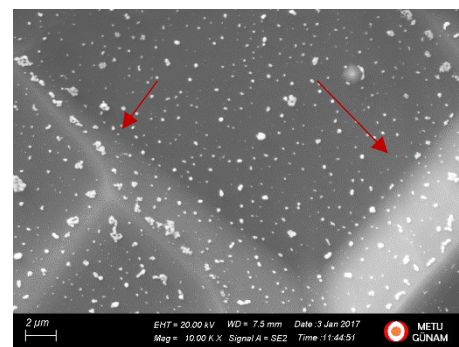
210 A



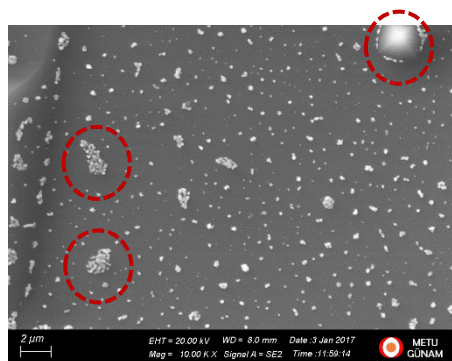
215 A



220 A



225 A



230 A

**Figure 5.28 SEM images of SET 2 (A parts, 10K Magnification)**

The SEM images of SET 2 (Figure 5.28) shows both the dispersion of particles and change in surface coverage caused by increasing number of spray passes. Marked areas indicate that the particles tend to settle on the edges of square-like structures or small pyramids. And by increasing number of spray passes, they start to cumulate like little clouds as happened at SET 1.

### 5.3.3 SEM Images for SET 3:

As it is in the other sets, it is seen that there are also small pyramids and square-like structures on this set. When the structures in this set are examined, it is determined that the deepest square-like structures and the most pointed pyramids are in this set. It can be seen how deep the structures are even in the SEM image viewed with no angle. (Figure 5.29) The "curve-anomalies" mentioned earlier in the reflection and diffuse reflection graphs are formed for this reason.

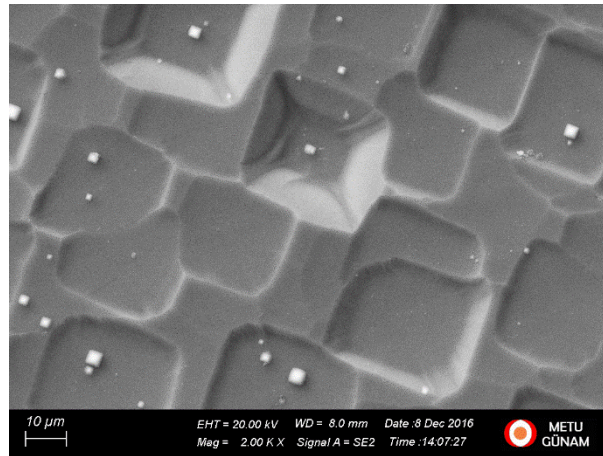


*Figure 5.29 SEM image of the reference (uncoated) device of SET 3 named 300A.*

Tilted SEM images are very important in terms of identifying squared-like structures and pyramids, if any, on the samples. With the help of these images, the behavior of the particles on the sample can be predicted or verified.

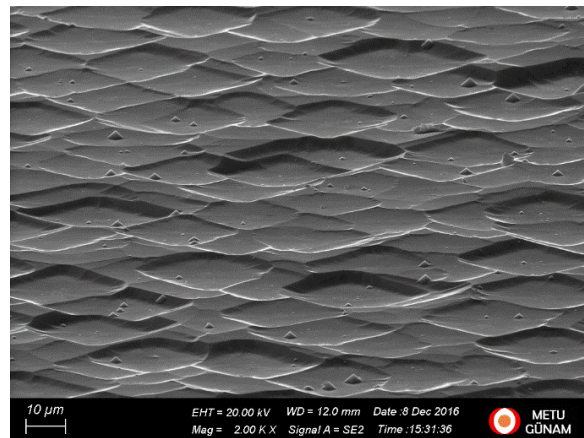
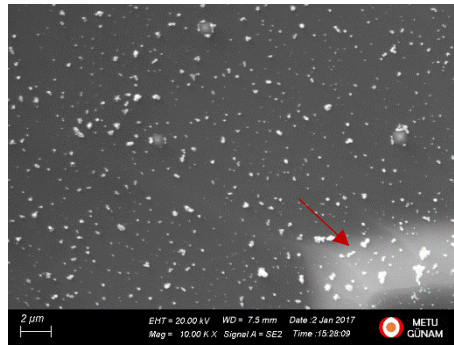


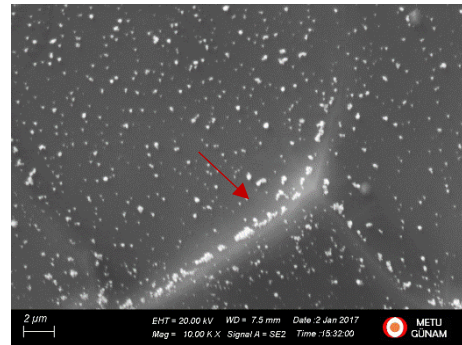
*Figure 5.30 SEM image of the reference (uncoated) device (300A) with 75° tilt.*

The Figure 5.30 points out the frequency of square-like structures and pyramids on the sample. As already mentioned, the deepest square-like structures and the most pointed pyramids are in this set. In the Figure 5.30, it is revealed how of en these structures are.

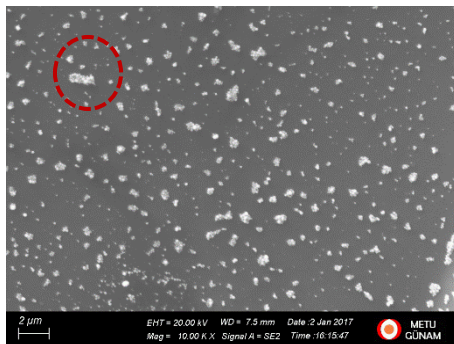
SEM images of coated devices, for observing the relation between number of spray passes and surface coverage, in ascending order in terms of number of spray passes;



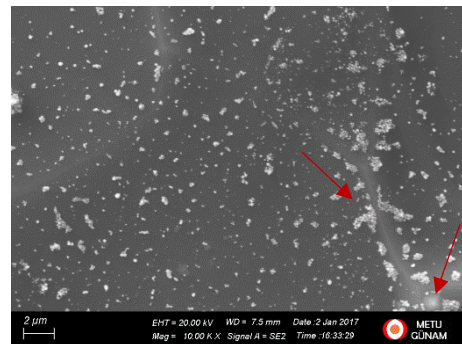
310 A



315 A



320 A



325 A



330 A

*Figure 5.31 SEM images of SET 3 (A parts, 10K Magnification).*

The pointed and the marked areas again gives an opinion about the particles behaviors. Deposits on corners and edges, cloud-like clusters were again observed. (Figure 5.31)

These information imply that no matter what the silicon nitride thicknesses are, particles behaviors are the same for all three sets; they are tend to cumulate with higher passes, and deposit near the edges and corners, depending on the structure of the solar cells.

#### 5.4 Solar Simulator Measurement Results:

Solar simulator measurements gives the most important data about this thesis; that is the efficiency of the solar cells. Before giving the change in efficiencies of the solar cells, the current-voltage graph of the devices will be shared to observe the effects of spray coating on I-V curves.

The effect of spray coating is coming from the optical enhancement through silver nanoparticles that coated on the solar cells.

As said in characteristics of PV chapter, the I-V curve of the solar cell is the superposition of the I-V curve of the solar cell diode in the dark with light generated current. [6]

By using silver nanoparticles' plasmonic properties; particles scattered the incident light and then enhanced the optical path length of the light inside the solar cell, the short circuit current value is increased, so the I-V curve of the samples are shifted-up.

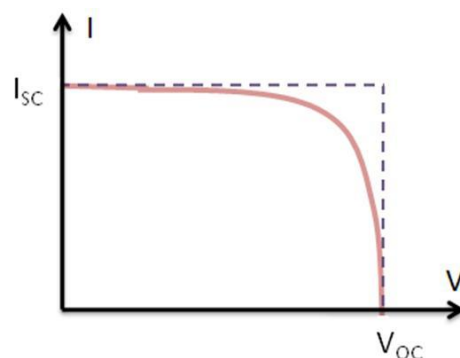


**Figure 5.32** Schematic Representation of Current-Voltage (I-V) Curve [41]

As can be seen at Figure 5.32, the maximum data point in y-axis is the  $I_{SC}$ , and when the value of  $I_{SC}$  increases, the curve is shifted-up.

#### 5.4.1 Current- Voltage Graphs of SET 1:

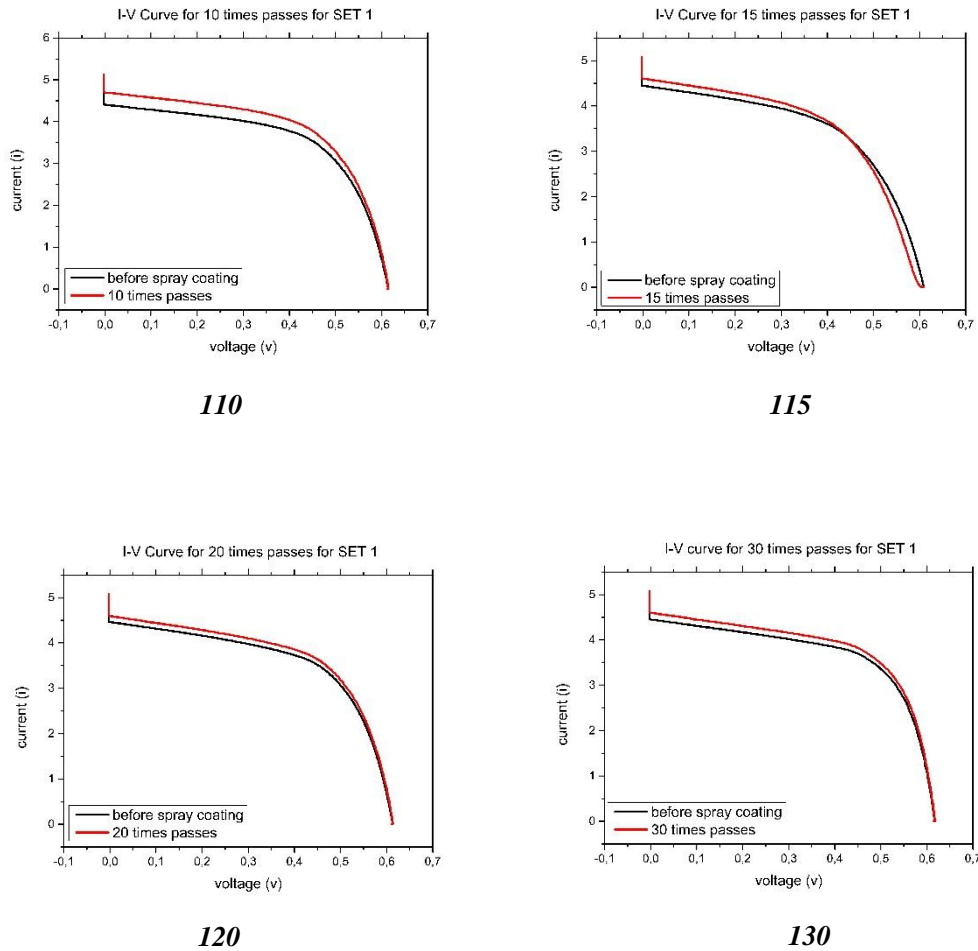


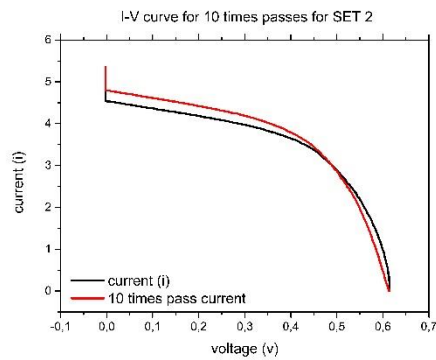
**Figure 5.33** Current-Voltage (I-V) Graphs of SET 1 before and after coating with silver nanoparticles

The red curves belong to the case after spray coating. The positive effect of spray coating, that discussed above, on the devices, can be easily observed. (Figure 5.33)

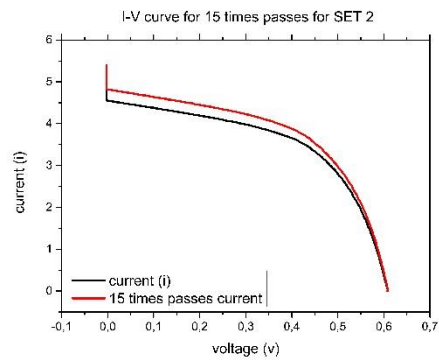
The greater effect belongs to the sample coated 10 times. (110)

Exact changes in  $I_{SC}$  values will be given in a table at the end of this part for all samples individually.

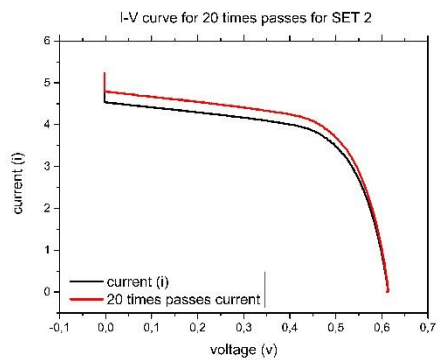
## 5.4.2 Current- Voltage Graphs of SET 2:



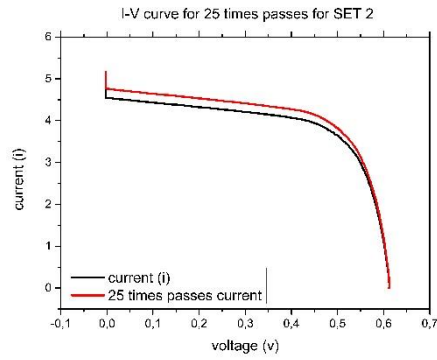
210



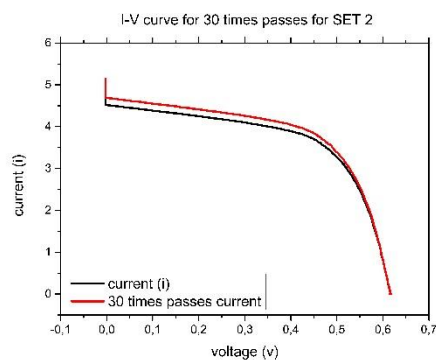
215



220



225

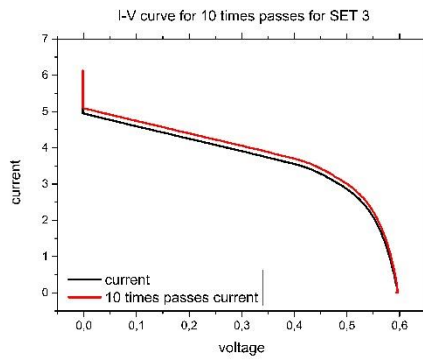


230

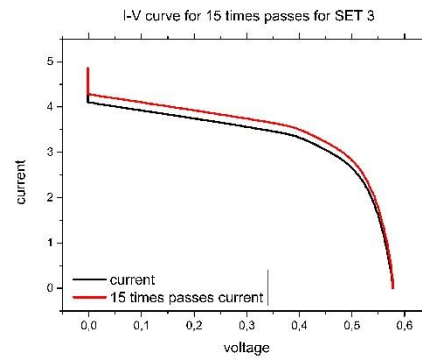
**Figure 5.34** Current-Voltage (I-V) Graphs of SET 2 before and after coating

Figure 5.34 indicates that spray coating technique has a positive effect on all samples. The red curves are again represents the case after spray coating. The greatest effect is seen on the sample that coated 15 times. (215)

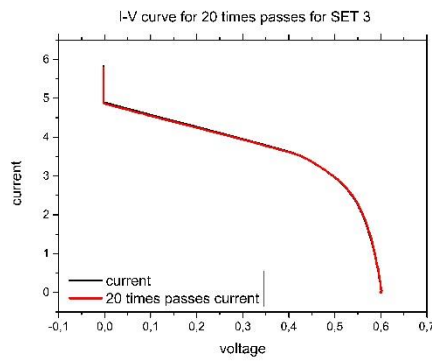
### 5.4.3 Current- Voltage Graphs of SET 3:



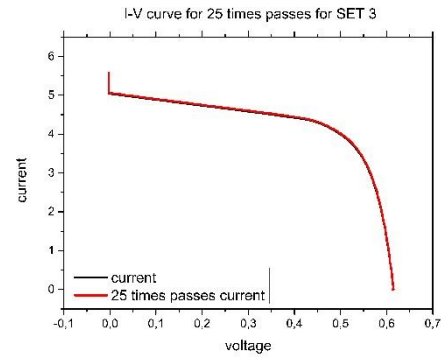
310



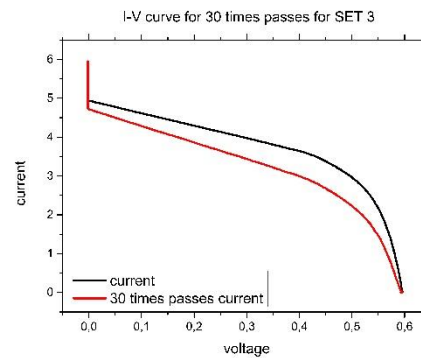
315



320



325



330

*Figure 5.35 Current-Voltage (I-V) Graphs of SET 3 before and after coating*

For this set, spray coating has a positive effect only on the samples that coated 10 and 15 times. If the curves of the samples that coated 20 and 25 times are examined, it can be say that there is neither a positive nor a negative effect provided by spray coating

technique. When the sample named 330 is taken into account, the change in curvature is clearly identified. The reason for this change is the increase in shunt losses.

Figure 2.7 gives the details of the changes that can occur in the IV curve. The increase in shunt losses means that there is a current leakage after the spray coating process. However, silver nanoparticles cannot cause current leakage, so the reason for this increase in shunt losses is likely to occur during laser cutting. Laser cutting can cause damage to the edges of the solar cell, and this damage may lead to a current leakage for this sample.

#### 5.4.4 Efficiency, Short Circuit Current ( $I_{sc}$ ), Open Circuit Voltage ( $V_{oc}$ ) and Fill Factor (FF) Values; before and after spray coating process:

**Table-1** Increase in  $\eta$  and change in F.F.,  $V_{oc}$  and  $I_{sc}$  of SET 1 ;

SET 1				
Cell name	efficiency	efficiency (a.c.)	efficiency (a.c.) 2 <sup>nd</sup> measurement	% increase
reference sample (uncoated)	8.78	--	--	--
10	10.06	10.7	10.67	6.36
15	9.3	9.63	9.64	3.55
20	10.04	10.36	10.3	3.19
25	15.07	14.53	14.5	-3.58
30	10.93	11.28	11.25	3.20

SET 1						
Cell name	F.F.	F.F. (a.c.)	$V_{oc}$	$V_{oc}$ (a.c.)	$I_{sc}$	$I_{sc}$ (a.c.)
reference sample (uncoated)	57.74	--	0.61	--	4.17	--
10	66.02	65.73	0.61	0.61	4.17	4.44
15	60.73	60.71	0.61	0.61	4.2	4.35
20	65.33	65.47	0.61	0.61	4.21	4.34
25	73.5	73.2	0.61	0.61	5.64	5.48
30	70.96	70.91	0.61	0.61	4.21	4.34

As seen from the Table-1, spray coating has nearly no effect on fill factor (FF) and open circuit voltage ( $V_{oc}$ ) as expected. As previously described in the characteristics of the photovoltaic devices part, the fill factor is a feature specified in the production stage that determines the quality of the device and the open circuit voltage is the highest voltage that can be obtained from a device and both of them cannot be changed by the spray coating.

It was observed that spray coating has a positive effect when considering the short circuit current ( $I_{sc}$ ). This effect is related to the reduction of the reflectance values of the solar cells. The short circuit current is inversely proportional to the reflectance values of the samples as mentioned earlier. As the surface is coated, the reflection values decrease and the short circuit current value increases.

The greatest effect of spray coating is observed on the efficiencies of the devices. In plasmonics part of the thesis, it is said that the metal nanoparticles that have a diameter of 50 nm and over scattering is the dominant property. (Figure 5.36)

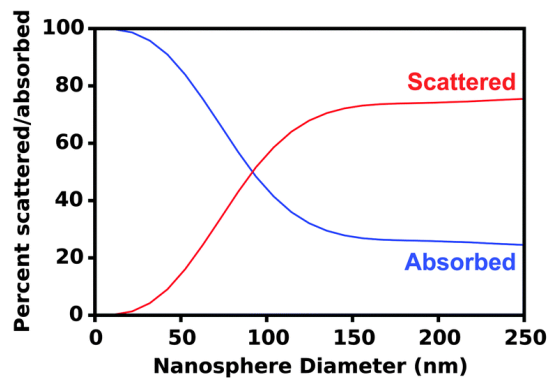


**Figure 5.36** Nanoparticles plasmonic behaviors with changing diameter [27]

It has been found through literature review that there has not been a study for increasing the efficiency of full-scale solar cells before. Thanks to this method, the efficiency of devices is increased even though the textured-like surfaces of the solar cells.

As described in the section on plasmonics, particles with a diameter of 50 nm and over (in this study between 100-130 nm) exhibit local surface plasmon resonance properties. A schematic representation of the LSPR is given again in Figure 5.37.

Thanks to the LSPR, the optical path length of the particles in the solar cell has been increased, so the efficiencies of the solar cells have increased.

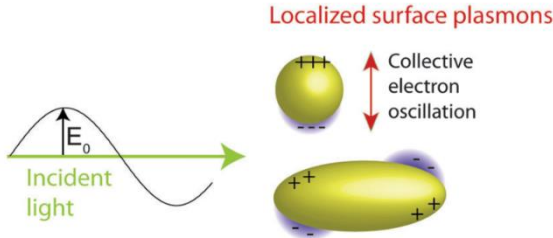


**Figure 5.37** Schematic of Localized Surface Plasmon Resonance [42]

Same principles and same comments are valid for the other sets, too. After giving the tables that includes the information about change in efficiency, fill factor, open circuit voltage and short circuit current; three sets will be compared to each other via "surface coverage vs. number of spray coating" and "surface coverage vs. increase in efficiency" graphs.

**Table-2** Increase in  $\eta$  and change in F.F.,  $V_{oc}$  and  $I_{sc}$  of SET 2;

SET 2				
Cell name	efficiency	efficiency (a.c.)	efficiency (a.c.) 2 <sup>nd</sup> measurement	% increase
reference sample (uncoated)	8.6	--	--	--
10	9.18	9.68	9.64	5.45
15	9.59	10.16	10.14	5.94
20	11.29	11.91	11.89	5.49
25	11.89	12.43	12.41	4.54
30	10.61	11.01	10.98	3.77

SET 2						
Cell name	F.F.	F.F. (a.c.)	V <sub>oc</sub>	V <sub>oc</sub> (a.c.)	I <sub>sc</sub>	I <sub>sc</sub> (a.c.)
reference sample (uncoated)	55.42	--	0.61	--	4.28	--
10	58.78	58.7	0.61	0.61	4.28	4.53
15	61.32	61.23	0.61	0.61	4.3	4.56
20	72.15	72.05	0.61	0.61	4.29	4.52
25	75.09	75.09	0.62	0.62	4.31	4.51
30	68.14	67.97	0.61	0.61	4.27	4.44

**Table-3** Increase in  $\eta$  and change in F.F., V<sub>oc</sub> and I<sub>sc</sub> of SET 3 ;

SET 3				
Cell name	efficiency	efficiency (a.c.)	efficiency (a.c.) 2 <sup>nd</sup> measurement	% increase
reference sample (uncoated)	7.79	--	--	--
10	9.75	10.21	10.18	4.71
15	9.34	9.92	9.88	6.20
20	10.11	10.67	10.68	5.54
25	13.05	13.86	13.83	6.21
30	10.1	7.82	7.82	-22.57

SET 3						
Cell name	F.F.	F.F. (a.c.)	V <sub>oc</sub>	V <sub>oc</sub> (a.c.)	I <sub>sc</sub>	I <sub>sc</sub> (a.c.)
reference sample (uncoated)	55.42	--	0.61	--	4.28	--
10	58.78	58.7	0.61	0.61	4.28	4.53
15	61.32	61.23	0.61	0.61	4.3	4.56
20	72.15	72.05	0.61	0.61	4.29	4.52
25	75.09	75.09	0.62	0.62	4.31	4.51
30	68.14	67.97	0.61	0.61	4.27	4.44

There is an exceptional situation in SET 3, sample 330. In current-voltage (I-V) curves section this situation is discussed and said that there is an increase in shunt current. So, the efficiency of this sample decreased despite spray coating.

### 5.5 Comparison of the Sets:

In this section; "surface coverage vs. number of spray coating" and "surface coverage vs. increase in efficiency" graphs of all sets will be given individually. However, for a meaningful comparison; "reflection, diffuse reflection and haze values over 400-1000nm spectral range" graphs (box charts) will be shared for each set.

Before going into deeper analysis, here is a brief information about how to read a box chart:

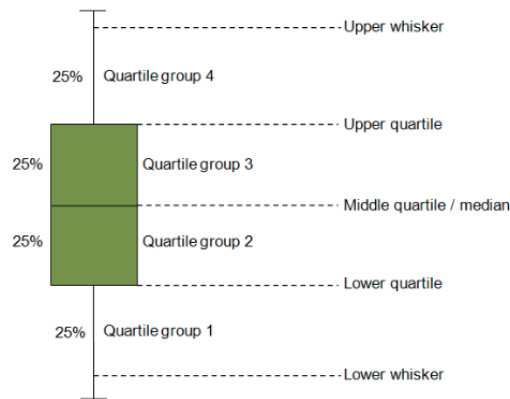


**Figure 5.38** Schematic of the reading a box chart [43]

Definitions of the terms;

*Median*: The mid-point of the data is called the median and it is the line that cuts the box into two parts. [43]

*Inter-quartile range*: the middle 50% of scores for the group is represented by the middle "box". [43]

*Upper quartile*: Seventy-five percent of the scores fall below the upper quartile.

*Lower quartile*: Twenty-five percent of scores fall below the lower quartile.

*Whiskers*: Scores/data outside the middle 50% are represented by the upper and lower whiskers. [43]

### 5.5.1 Relation between surface coverage rates and the number of spray passes for all sets:

The surface coverage rate vs. number of spray passes graphs give an opinion about the effects of shadows that caused reduction of increase in efficiency. Also this graphs play very important roles for this thesis because the aim of this thesis is to fall below to 10% of the surface coverage rate for observing the plasmonic effects. By examined following graphs, relation between the rate of surface coverage and increasing number of passes can be determined.

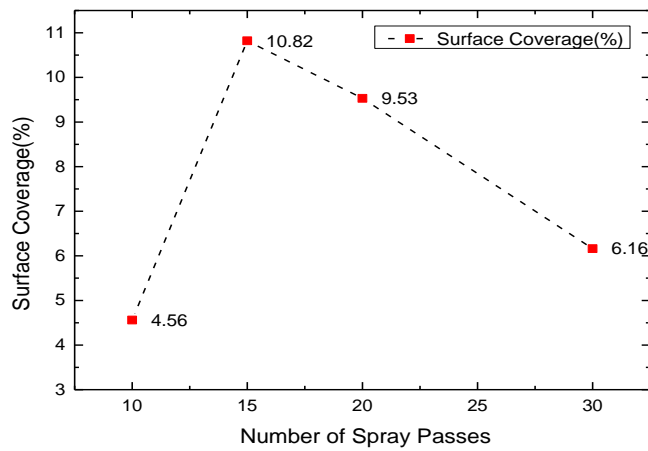


**Figure 5.39** Surface coverage (%) vs. Number of Spray Passes for SET 1

*(The line is a guide for the eyes.)*

When the Figure 5.39 is examined, it is seen that the aim is fulfilled. The reason of the decrease in surface coverage rate with increasing number of spray passes is that the sharpest edges of the square-like structures or the tips of the pyramids repelled particles sprayed on when the number of passes increased.

Actually, for each case; the surface coverage rate is around or below 10%, as aimed at the beginning. This achievement can be seen from following graphs;

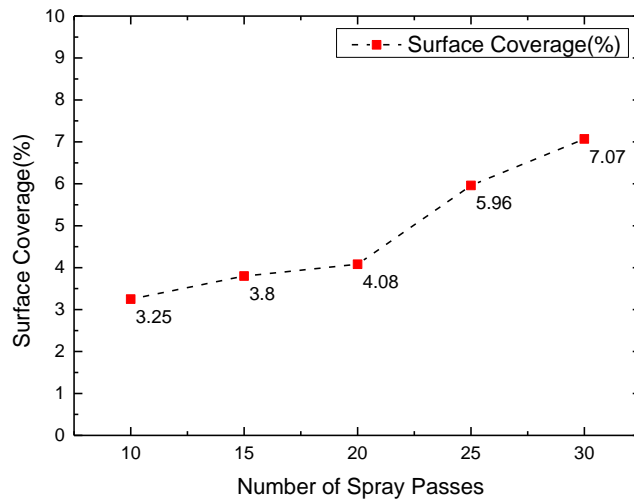


**Figure 5.40** Surface coverage (%) vs. Number of Spray Passes for SET 2  
 (The line is a guide for the eyes.)

For SET 2, there is a direct proportional relation between number of spray passes and surface coverage (%) rates. (Figure 5.40) This relation suggests that the square-like structures and pyramidal defects have less impact on SET 2 than SET 1. This suggestion is supported by SEM images of SET 2. (Figure 5.28)

So far, also by the help of this information, the idea that spray coating technique works best on SET 2 is supported.

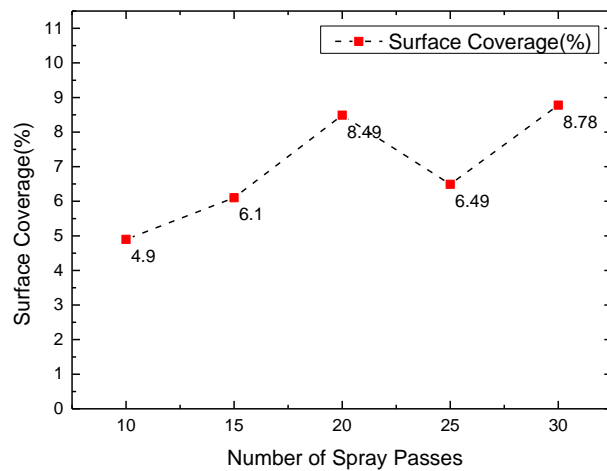


**Figure 5.41** Surface coverage (%) vs. Number of Spray Passes for SET 3  
 (The line is a guide for the eyes.)

When Figure 5.41 is examined, if 25 times coated sample (325) is removed, the same tendency in Figure 5.40 is seen here. Given the removal of 325 from the set, the correct ratio between the number of spray passages and the surface coverage (%) rates can be seen. Figure 5.31 shows the dispersion of the particles on the surfaces of solar cells. The clustering (overlapping) of particles in 325 is higher than 320 (sample coated 20 times), and hence the surface coverage (%) of 325 is less than 320.

At the end, as said earlier, for all three sets the goal of the thesis in terms of the rate of surface coverage is achieved.

### 5.5.2 Relation between increase in efficiency (%) and surface coverage (%) for all sets:

The graph of increase in efficiencies vs surface coverage (in percentage scale) is given below.

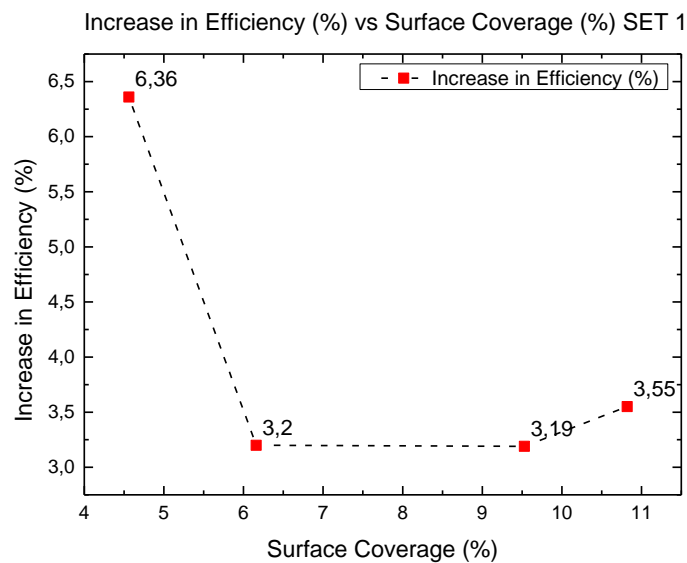


**Figure 5.42** Increase in efficiency (%) vs. Surface Coverage (%) for SET 1  
(The line is a guide for the eyes.)

When the graph is examined, it is observed that the increase in the percentages of efficiencies has decreased after 5% of surface coverage. This result indicates that increase in surface coverage (%) resulting decrease in “increase in efficiency” of solar cells. (Figure 5.42)

This decrease can be explained by the increase in the number of spray passes which is causing the particles to overlap. The particles that overlapped made clusters and they began to create shadows. (Figure 5.24) Moreover, these clustering (agglomerated) particles inhibited the formation of localized particle plasmon resonance. (Figure 5.37)

As a result, an increase in the efficiency of each solar cells in this set was achieved with spray coating technique. The increase in efficiency of the solar cell that has a 5% surface coverage is about six percent while it is around three percent for the cell that has an 11% surface coverage.

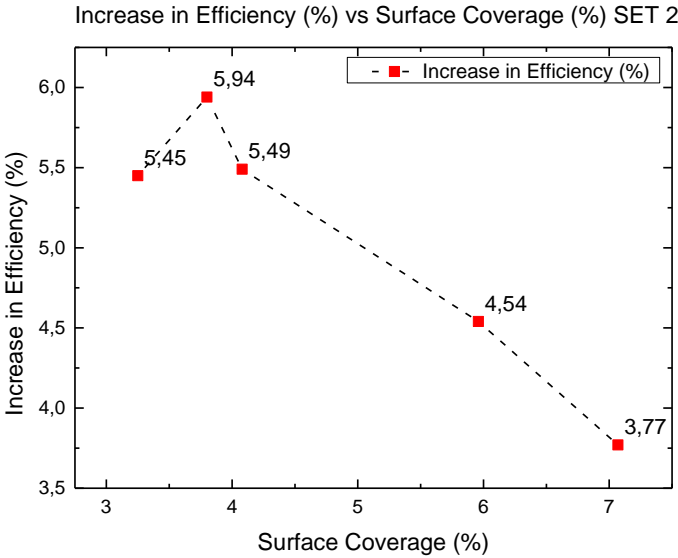


**Figure 5.43** Increase in efficiency (%) vs. Surface Coverage (%) for SET 2  
*(The line is a guide for the eyes.)*

Figure 5.43 gives the relation between increase in efficiency (%) and surface coverage (%) for SET 2. As can be seen from the graph, again after 5% surface coverage rate, increase in efficiency (%) values decrease. The reason for this reduction is the same as described in the first set. As the number of spray passes increases (resulting in increase in surface coverage), the particles tend to overlapped and settled on the edges of the square-liked structures, as can be seen from the SEM images. (Figure 5.30) This tendency is hampering the formation of the LSPR.

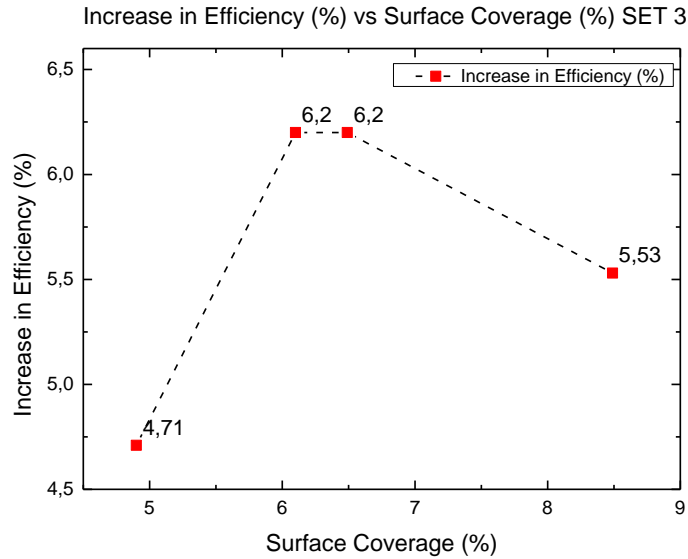


**Figure 5.44** Increase in efficiency (%) vs. Surface Coverage (%) for SET 3

*(The line is a guide for the eyes.)*

When Figure 5.44 is examined, it is seen that there is missing data point. This point belongs to the sample that 30 times coated (330). The reason for this is the shunt resistance in that solar cell. Shunt resistance causing the reduction of the efficiency of this cell as described in the current-voltage curves section. This decrease is given in Table-3. Again for SET 3, after 5% surface coverage rate, the increase in efficiency of the solar cells decreases. The maximum increase in efficiency is around 6.2% and the minimum is around 4.71%.

When all sets are considered, it is seen that the spray coating technique works best on the second set if the average increases for all sets are considered.

### 5.5.3 Reflection, Diffuse Reflection and Haze Analysis for all sets:

As indicated at the beginning of this chapter, it is more meaningful to give the graphs of “increase in efficiency vs. number of spray passes” and the “integral reflection, diffuse reflection and haze values over 400-1000nm spectral range” graphs together to better understand the relationship between the graphs.

At first, “Integral Reflectance Values over 400-1000nm Spectral Range vs. Sample Position & Number of Spray Passes” graphs for all sets are shared.

These graphs also include the linear fit of the plot drawn by calculating the mean values of the samples from regions A, B and C for each spray coating. These fits give an idea about the trend in the graphs.

Figure 5.45, 5.46 and 5.47 are as follows:

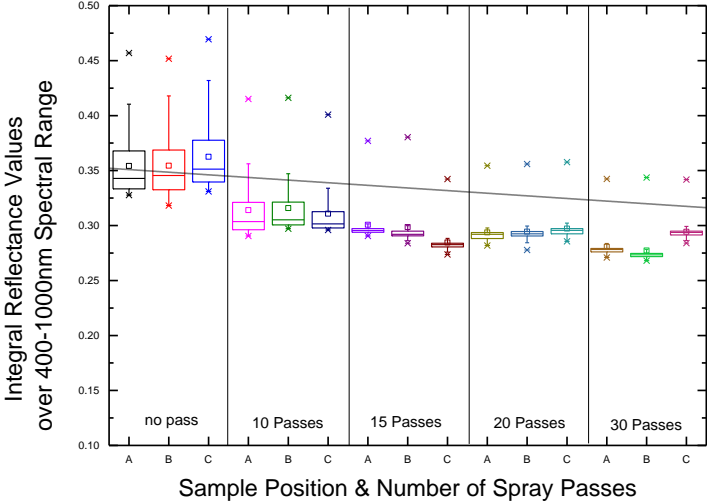


**Figure 5.45** Integral Reflectance values over 400-1000 nm Spectral Range vs. Sample Position & Number of Spray Passes for SET1.

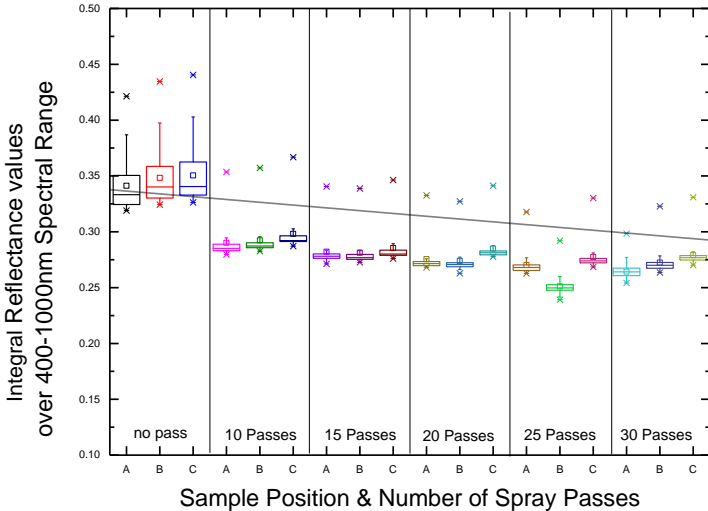


**Figure 5.46** Integral Reflectance values over 400-1000 nm Spectral Range vs. Sample Position & Number of Spray Passes for SET2.

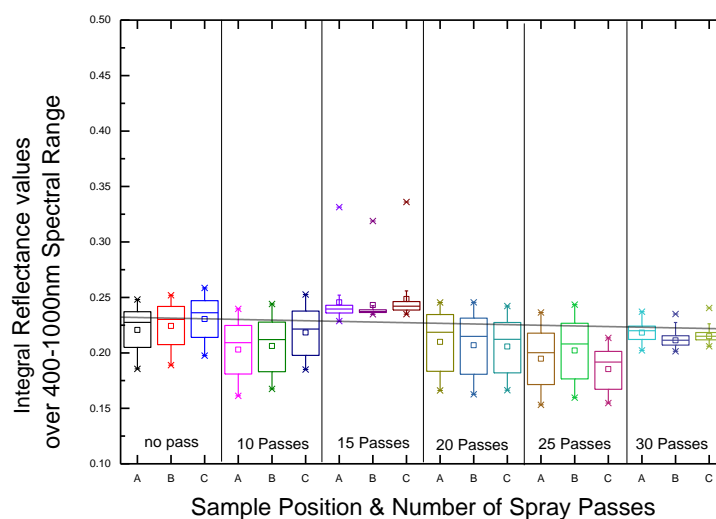


**Figure 5.47** Integral Reflectance values over 400-1000 nm Spectral Range vs. Sample Position & Number of Spray Passes for SET3.

Information coming out of examining the integral reflectance values graphs for all three sets;

- When the blocks examined individually, the homogeneity of the spray coating can be clearly seen for all sets. Each block containing three boxes for three parts of the cell (A, B and C), has the reflectance values that are nearly the same. This means that the center, the edges and the corners of the solar cells were evenly coated by spray gun.
- The linear fit implies that increase in number of spray passes leads to decrease in reflectance values, as desired.
- There is a nearly 35% of reduction in reflectance values, if uncoated samples and samples coated 30 times are compared for SET 1 and SET 2. As mentioned earlier, there is a different situation for SET 3's reflection measurement data. Maybe there was a problem in doping or metallization step of the production to cause this situation. At the end of this section in EQE results part, this problem will be seen and discussed more clearly.

The second graph sets are “Diffuse Reflectance values over 400-1000nm Spectral Range vs. Sample Position & Number of Spray Passes” for all three sets.

These graphs are also including the linear fit of the plot drawn by calculating the mean values of the samples from regions A, B and C for each spray coating.

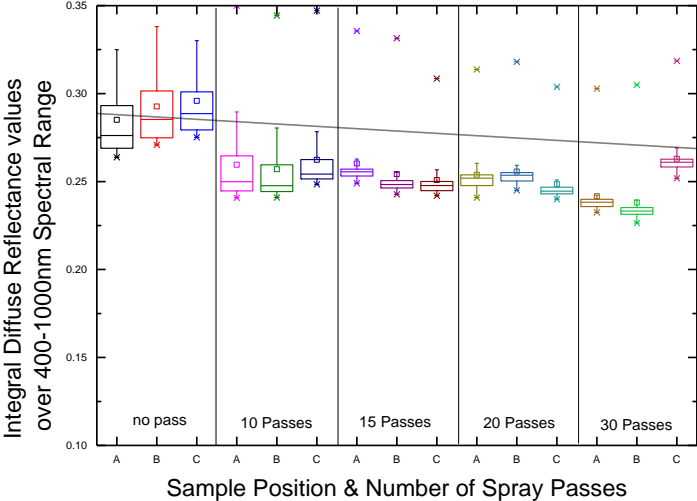


**Figure 5.48** Integral Diffuse reflectance values over 400-1000 nm Spectral Range vs. Sample Position & Number of Spray Passes for SET1.

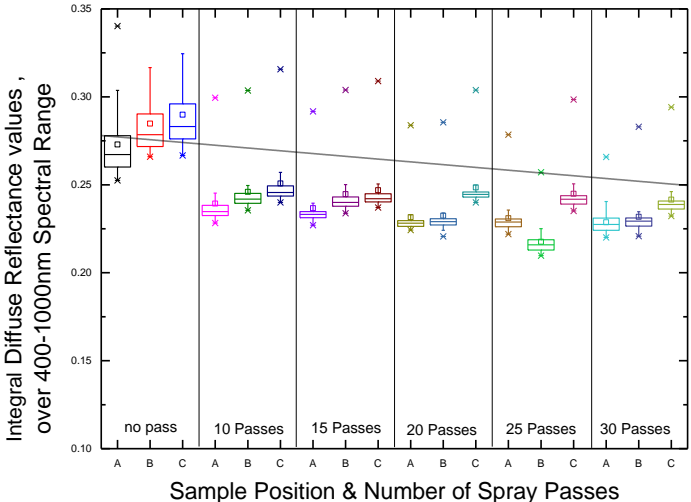


**Figure 5.49** Integral Diffuse reflectance values over 400-1000 nm Spectral Range vs. Sample Position & Number of Spray Passes for SET2.

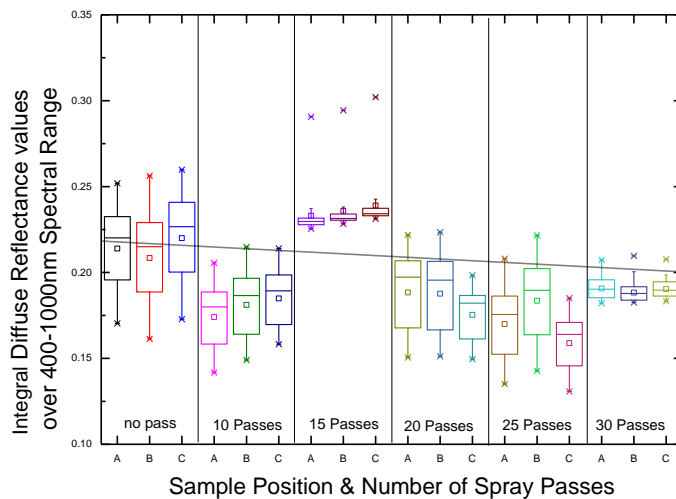


**Figure 5.50** Integral Diffuse reflectance values over 400-1000 nm Spectral Range vs. Sample Position & Number of Spray Passes for SET3.

Aforementioned study on flat silicon wafers showed that the number of spray passes and diffuse reflectance values are directly proportional to each other. Furthermore, for earlier studies; the haze values and the change in efficiency values are thought to be in harmony, and the optical effects of the particles on the efficiency of the solar cells were investigating considering this fact.

However, in this study as shown in Figure 5.48, 5.49 and 5.50, there is an inversely proportional relation between number of spray passes and diffuse reflectance values. Even there is a correlation between increase in efficiency (%) graphs and integral diffuse reflectance values over 400-1000nm spectral range graphs. So, when the change in efficiency values (%) of solar cells are examined, not only the change in haze values (%) but also change in diffuse reflectance values must be taken into account after that fact has emerged.

For example, when Figure 5.39 and 5.40 are considered, the trends in the change in efficiency (%) data are similar to linear fits in Figure 4.48 and 4.49, which is the supportive information of above discussion. Even for SET 3, although this set seems to be problematic, there is a correlation between the change in efficiency (%) graph (Figure 5.41) and diffuse reflectance graph of SET 3. (Figure 5.50)

Next, “Haze values (%) over 400-1000nm Spectral Range vs. Sample Position & number of Spray Passes” graphs for all three sets are given. The linear fits are drawn again for these graphs, too.

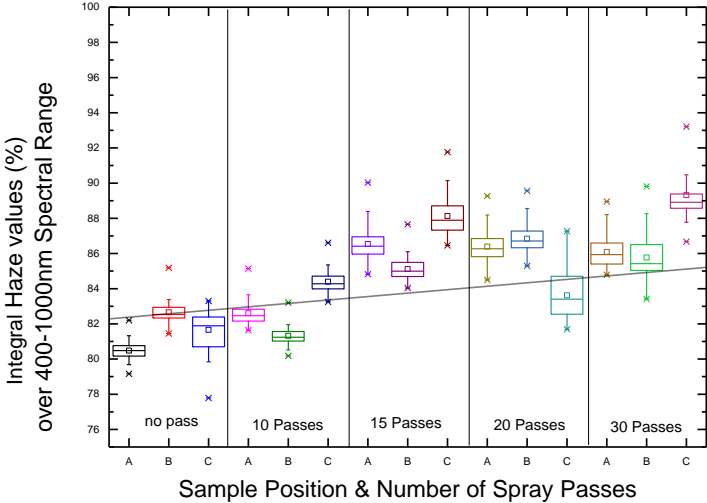


**Figure 5.51** Integral Haze values (%) over 400-1000 nm Spectral Range vs. Sample Position & Number of Spray Passes for SET1.

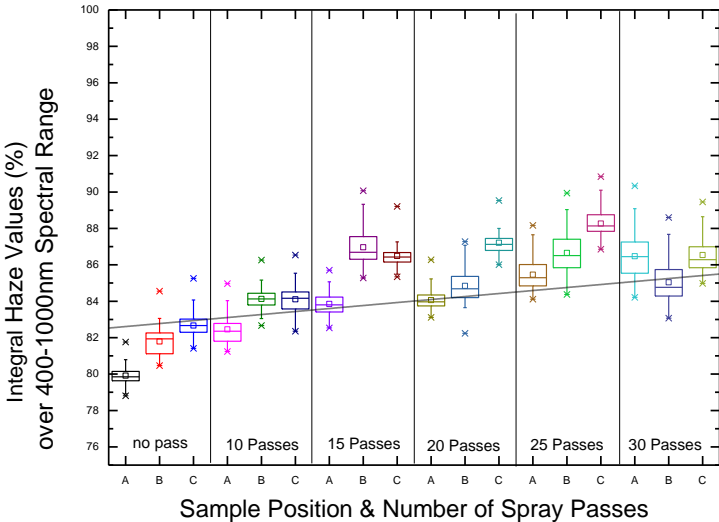


**Figure 5.52** Integral Haze values (%) over 400-1000 nm Spectral Range vs. Sample Position & Number of Spray Passes for SET2.

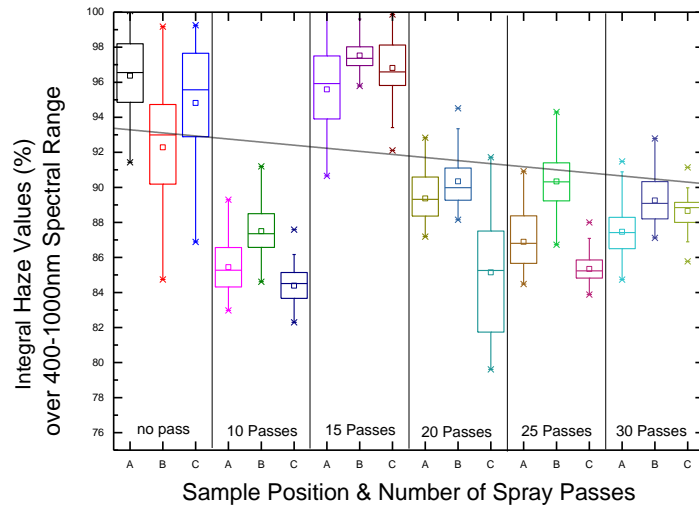


**Figure 5.53** Integral Haze values (%) over 400-1000 nm Spectral Range vs. Sample Position & Number of Spray Passes for SET3.

When Figures 5.39 and 5.40 are compared with Figure 5.51 and 5.52, it is seen that the trends in “increase in efficiency” graphs and “the linear fits to haze values” graphs are opposite to each other. Again, the discussion above is proved.

Again for SET 3, the dispersion of the data in Figure 5.53 is different from Figure 5.51 and 5.52 as expected. It is known that the haze values are calculated through the reflection and diffuse reflection values, the anomaly on the graph of the haze values (%) of SET 3 is not surprising.

The hazes of the devices are between 80-90 %. These results correct that the surfaces of the solar cells are not flat and most of the illuminated light diffused by the surface. In terms of industrial produces, these results are more accurate than flat surfaces' results because it is not yet possible to produce flat silicon solar cells with today's technology.

## 5.6 Quantum Efficiency Measurement Results:

As explained in detail at Chapter 2, quantum efficiency of a solar cell is the possibility that an incident photon of energy  $E$  will transport one electron to the external circuit. [5]

External and internal quantum efficiencies (EQE & IQE) are differ from each other in terms of reflectivity of the solar cell.

Below IQE graphs are drawn accordion to this equation;

$$IQE = \frac{EQE}{1 - R_{total}} \quad (5.1)$$

The external quantum efficiency of the solar cell is a value that emerges during the production stage of the cell. But the internal quantum efficiency is calculated by Equation 5.1 and is affected by the change in reflectivity of the cell. That is, the effect expected to occur in this study is related to internal quantum efficiency. However, the effect on the quantum efficiency values of the spray coating cannot be clearly observed since the quantum efficiency measurements cannot be made before spray coating. This is because the samples must be smaller than the full size so that the measuring system can be used correctly during the EQE measurement. But breaking the samples before the spray coating step causes both the coating step and the solar simulator measurement step to be troublesome. So, EQE measurements can only be made after spray coating and solar simulator measurement steps.

As a result, it is thought that the fluctuations in the graphs below are due to the characteristics that appear during the production stage of the solar cells.

Measurements showed that quantum efficiency values in the solar cells with a thin silicon nitride layer (SET 1, Figure 5.54) are progressively decreasing from the center of the cell to the edges and corners. The difference is reduced when the silicon nitride thickness reaches the middle level. (SET 2, Figure 5.56) In order to support this argument, the box chart analysis of both EQE and IQE are given for all three sets.

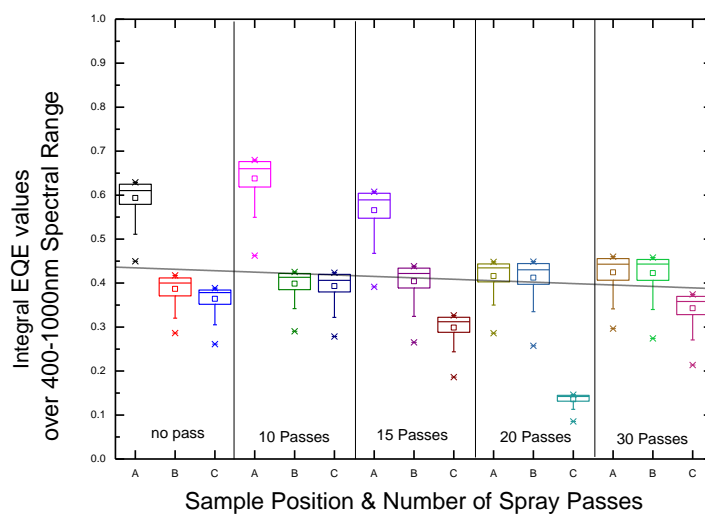


**Figure 5.54** Integral External Quantum Efficiency Values over 400-1000 nm Spectral Range vs. Sample Position & Number of Spray Passes for SET1.

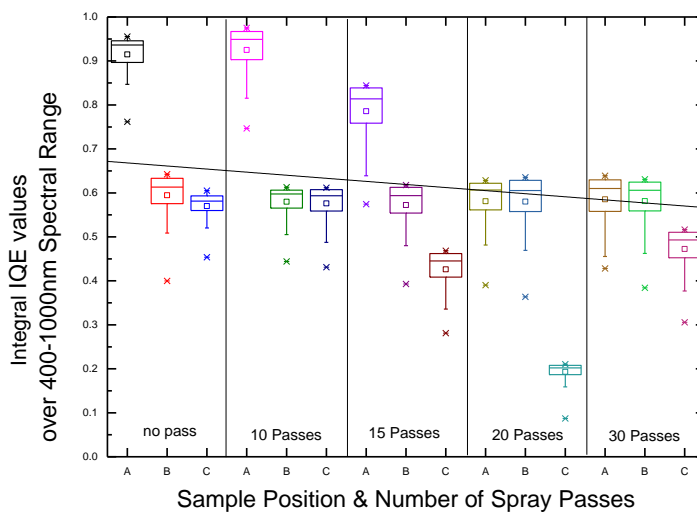


**Figure 5.55** Integral Internal Quantum Efficiency Values over 400-1000 nm Spectral Range vs. Sample Position & Number of Spray Passes for SET1.

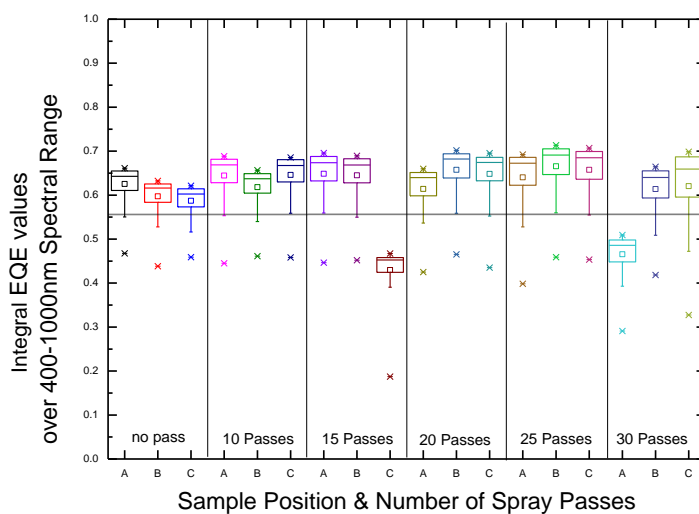


**Figure 5.56** Integral External Quantum Efficiency Values over 400-1000 nm Spectral Range vs. Sample Position & Number of Spray Passes for SET2.

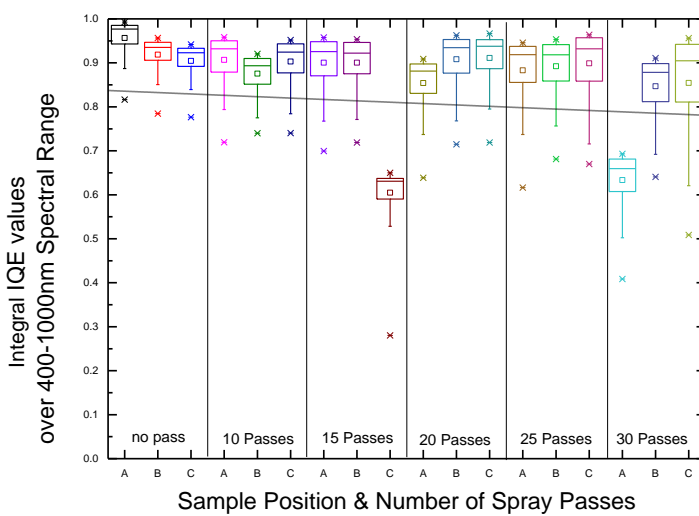


**Figure 5.57** Integral Internal Quantum Efficiency Values over 400-1000 nm Spectral Range vs. Sample Position & Number of Spray Passes for SET2.

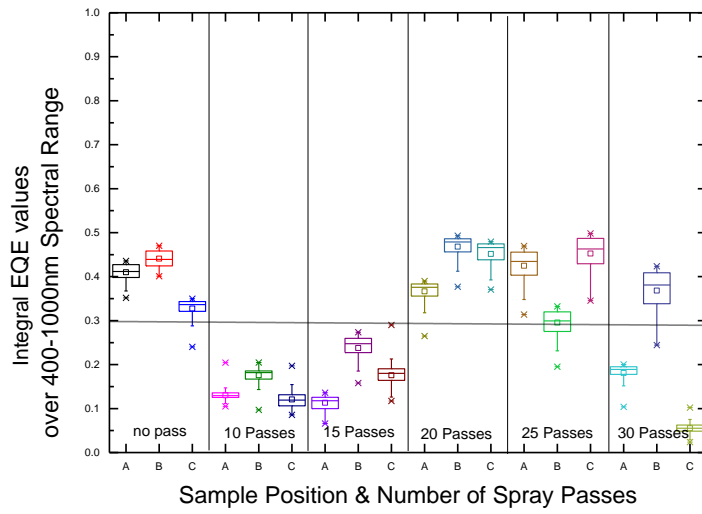


**Figure 5.58** Integral External Quantum Efficiency Values over 400-1000 nm Spectral Range vs. Sample Position & Number of Spray Passes for SET3.

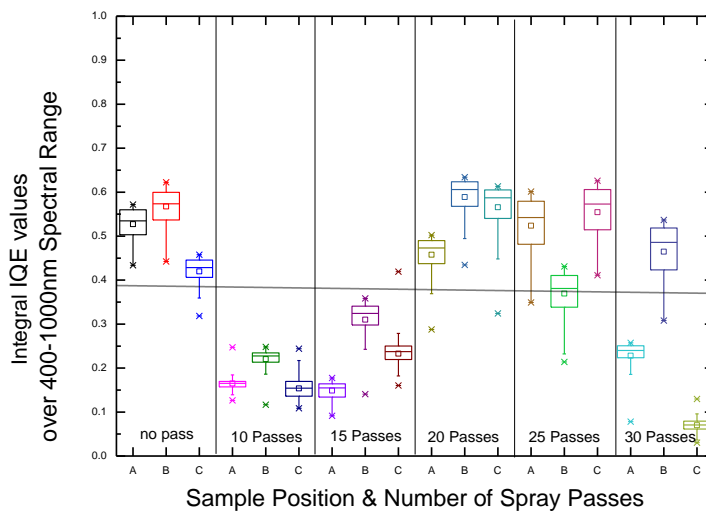


**Figure 5.59** Integral Internal Quantum Efficiency Values over 400-1000 nm Spectral Range vs. Sample Position & Number of Spray Passes for SET3.

When Figure 5.54 is examined, the differences in EQE values between A, B and C parts (center, edges and corners) of the solar cell can be observed. If Figure 5.54 and 5.55 are compared, the effect of the spray coating be seen via the linear fit and the increase in IQE values (with decreasing reflectance values), at Figure 5.55.

In reflectance, diffuse reflectance and solar simulator measurements results, it was suggested that the spray coating technique works best on SET 2. Figure 5.56 and 5.57 supports that suggestion. In Figure 5.56 it is clearly seen that samples in SET 2 starts the race in one step forward because they are already working well comparing to other sets. And when Figure 5.57 is examined, the IQE values reaches nearly 1, which is the expected outcome to fulfill after spray coating.

It was said that the results of the samples in SET 3 were worse than the results of the samples in other sets while the whole measurement results were being shared till now.

The reason for this difference has arisen during quantum efficiency measurements. Figure 5.58 shows that the samples of this set do not work well due to the problems arising from the production phase. So in Figure 5.59 the effect of spray coating is observed only with the increase of IQE values.

## 5.7 The “125” case:

As mentioned at results and discussion part, the sample named "125" was omitted from the results of SET 1. It was said that the reason for this would be explained at the end.

The reason for omitting the results coming out of 125 was shown itself in SEM imaging step. A small confusion was made before starting the experiment, a different sample was given from the SET 1. In SEM imaging step the following image appeared;

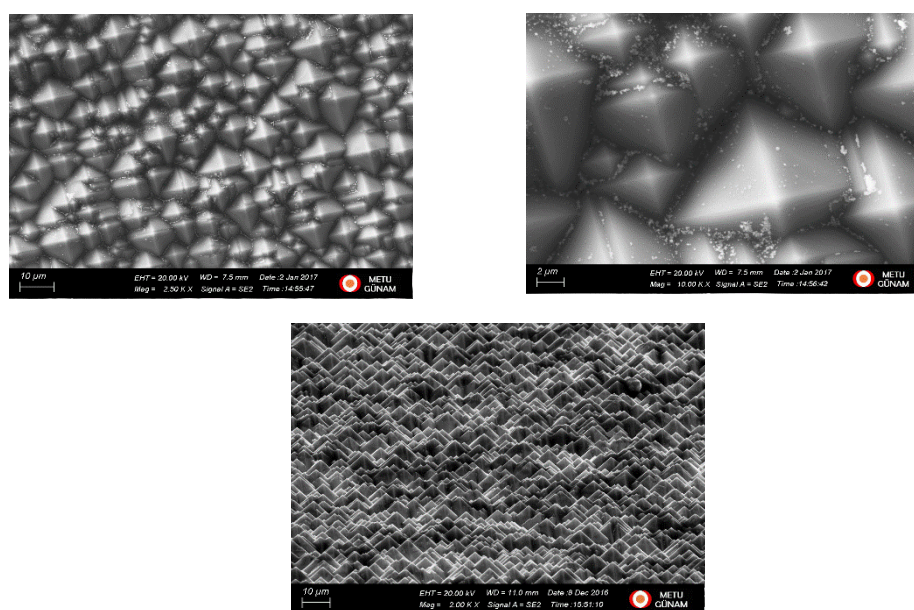


**Figure 5.60** SEM image of the sample named 125 a- 2.5 K b-10.00K and c- 2.00K with 75° tilt

As can be seen from the Figure 5.60, the sample 125 has pyramidal textured surface. This image answers all the questions about this sample.

The biggest problem with devices with pyramidal textured surfaces is poor passivation at the corners and tops of the pyramids. So these parts of the device do not work very well. During spray coating, nanoparticles were deposited on these corners/edges as shown in Figure 5.60.

A nanoparticle is added to the already bad passivated area and also create shadows. Moreover, these overlapped nanoparticles cannot use the LSPR properties. For these reasons the results of this sample were removed from the sets.

But this sample is a valuable example because it demonstrates that spray coating techniques should not be used on samples with pyramidal textured surfaces.



## CONCLUSIONS

In this thesis, the main goal is to increase the efficiencies of full scale silicon solar cells. For this purpose, the plasmonic properties of metal nanoparticles were utilized. First, a colloidal silver nanoparticle solution was produced using the polyol technique. With the help of a spray gun, the colloidal solution was sprayed onto the surfaces of full-size sunscreens. After the spray coating phase, the surfaces were heat treated to form a plasmonic interface. These interfaces were created by using the LSPR properties of silver nanoparticles having diameters of 100 nm and above, as previously described. Thanks to the LSPR properties, these particles on the surface are interacted with incoming light and scattered the light. This scattering increases the optical path length of the incident light in the solar cell, thus allowing for an improvement in the efficiency of the solar cells.

In this study, the factors that will affect the LSPR mechanism, and therefore the efficiency of the solar cells, are discussed. For this discussion to be made, firstly silicon solar cells were produced in three different silicon nitride thicknesses. These thicknesses are 5-10 nm, 10-15 nm and 18-20 nm, respectively. The investigation of the silicon nitride thickness is intended to investigate how well the plasmonic activities of silver nanoparticles are affected by the antireflection coating layer. The previously mentioned study named "self-organized fabrication" has shown that the thick silicon nitride layer inhibits the plasmonic effects. In this study, the results showed that the best system is the system which has 10-15nm silicon nitride layer, so called SET 2.

The second step to investigate the factors that affect LSPR mechanism is changing the number of spray passes. Before starting to work with solar cell, there was a trial on silicon wafers to determine the number of spray passes. This trial indicates that the number of spray passes should be 10-15-20-25 and 30 in order cover the 10% of the surfaces of the solar cells. The ratio, that is 10%, is a very important information because it is the ideal ratio for light management in the solar cell.

The results of the steps described above to determine the factors affecting / enhancing the efficiency of the solar cells were found via the reflection, diffuse reflection, and quantum efficiency measurements and solar simulator.

The results are very promising. The average surface coverage rate is 6.42% regardless of silicon nitride thicknesses. As mentioned earlier that the ideal ratio for better photon management is 10% or below, hence this study provided an ideal surface coverage. It is seen that this work has a positive effect on increasing the efficiency of the solar cells. By creating plasmonic interfaces, the efficiency of the solar cells have been increased  $6\pm 2\%$ .

The sample that have pyramidal textured surface showed that spray coating technique did not work well on that kind of surfaces. In future studies, this information should be taken into account.

The experimented solar cells are full scale and have roughness due to the saw damage etching on their surfaces. Considering these facts, it is seen that these results are very important for future studies.

As a result, by spray coating the colloidal silver nanoparticle solution onto silicon solar cells, there is a remarkable increase in efficiency of the solar cells.

In the future if this technique is developed, the increase in efficiency values will be higher than this study. Even the Shockley-Queisser limit can be exceeded by developing this study. For example by changing the production steps of the solar cells, the silver nanoparticles can be used inside the cell, or instead of silver nanoparticles, silver nanorods can be used to decorate the solar cells' surfaces.

## REFERENCES

- [1] W. Shockley, H. Queisser, and H. J. Queisser, “The Shockley-Queisser limit,” *J. Appl. Phys.*, vol. 32, pp. 510–519, 1961.
- [2] A. N. Sprafke and R. B. Wehrspohn, “Current Concepts for Optical Path Enhancement in Solar Cells,” pp. 1–20, 2015.
- [3] M. Zolfaghari Borra *et al.*, “A feasibility study for controlling self-organized production of plasmonic enhancement interfaces for solar cells,” *Appl. Surf. Sci.*, vol. 318, pp. 43–50, 2014.
- [4] A. Arango *et al.*, “Influence of the Substrate on the Morphology of Self-Assembled Silver Nanoparticles by Rapid Thermal Annealing,” *J. Phys. Chem. C*, vol. 120, no. 32, pp. 18235–18242, 2016.
- [5] J. Nelson, “The Physics of Solar Cells,” *Prog. Semicond. Mater.*, p. 384, 2003.
- [6] S. Honsberg, Christiana; Bowden, “PV Education.” [Online]. Available: [www.pveducation.org](http://www.pveducation.org). [Accessed: 01-Jan-2016].
- [7] S. Sharma, K. K. Jain, and A. Sharma, “Solar Cells: In Research and Applications—A Review,” *Mater. Sci. Appl.*, vol. 6, no. 12, pp. 1145–1155, 2015.
- [8] “Types of Crystalline Solar Cells.” [Online]. Available: <http://www.tindosolar.com.au/learn-more/poly-vs-mono-crystalline/>. [Accessed: 01-Jan-2017].
- [9] “Innovation: Thin Film Solar Cells,” *Materia*, 2016. [Online]. Available: <https://materia.nl/article/innovation-thin-film-solar-cells-at-mx2016/innovation-thin-film-solar-cells-at-mx2016-1/>.
- [10] “Create Greener Organic Solar Cells,” 2014. [Online]. Available: <https://plus.google.com/communities/111183346112172462411>. [Accessed: 01-Jan-2017].
- [11] LARGENT & WENHAM, “Understanding the p-n Junction,” in *UNSW Photovoltaics*, 2012, pp. 13–24.
- [12] T. Markvart and L. Castaier, “Principles of Solar Cell Operation,” *Sol. Cells*, pp. 3–25, 2013.
- [13] L. Abbot, Derek; White, “Solar IV Curve Theory,” 2014. [Online]. Available: <http://eleceng.adelaide.edu.au/>. [Accessed: 01-Jan-2016].
- [14] “Interpreting I-V Curve Deviations.” [Online]. Available: <http://solarprofessional.com/articles/operations-maintenance/interpreting-i-v-curve-deviations>. [Accessed: 01-Jan-2017].
- [15] C. Riordan and R. Hulstron, “What is an air mass 1.5 spectrum? [solar cell performance\ncalculations],” *IEEE Conf. Photovolt. Spec.*, pp. 1085–1088, 1990.

- [16] P. By, “World ’ s largest Science , Technology & Medicine Open Access book publisher First-Transition Metal Oxocomplex – Surface-Modified Titanium ( IV ) Oxide for Solar Environmental Purification.”
- [17] B. Soediono, “Photovoltaic (PV) materials and devices,” *J. Chem. Inf. Model.*, vol. 53, p. 160, 1989.
- [18] K. Yu and W. Walukiewicz, “A Step Closer to the Optimum Solar Cell,” *Science Beat Berkeley LAB*, 2004. [Online]. Available: <http://www2.lbl.gov/Science-Articles/Archive/sb-MSD-multibandsolar-panels.html>.
- [19] T. Schmidt, “Using Moleculesto Capture Solar Energy,” 2016. [Online]. Available: <http://slideplayer.com/slide/7851490/>. [Accessed: 01-Jan-2017].
- [20] M. Fathi, A. Mefoued, A. Messaoud, and Y. Boukennous, “Cost-effective photovoltaics with silicon material,” *Phys. Procedia*, vol. 2, no. 3, pp. 751–757, 2009.
- [21] IRENA (Inernational Renewable Energy Agency) and IRENA, *the Power To Change: Solar and Wind Cost Reduction Potential*, no. June. 2016.
- [22] Institute for Solar Energy Systems, “Photovoltaics Report,” *Fraunhofer*, 2016.
- [23] P. Manley, S. Burger, F. Schmidt, and M. Schmid, “Design Principles for Plasmonic Nanoparticle Devices,” *arXiv Prepr. arXiv1403.7919*, pp. 1–29, 2014.
- [24] L. Novotny and B. Hecht, *Principles of Nano-Optics*, vol. 1, no. 4. 2006.
- [25] M. Li, S. K. Cushing, and N. Wu, “Plasmon-enhanced optical sensors: a review.,” *Analyst*, vol. 140, pp. 386–406, 2014.
- [26] D. D. Evanoff and G. Chumanov, “Synthesis and optical properties of silver nanoparticles and arrays,” *ChemPhysChem*, vol. 6, no. 7, pp. 1221–1231, 2005.
- [27] W. R. Erwin, H. F. Zarick, E. M. Talbert, and R. Bardhan, “Light trapping in mesoporous solar cells with plasmonic nanostructures,” *Energy Environ. Sci.*, vol. 9, p. , 2016.
- [28] M. A. Green and S. Pillai, “Harnessing plasmonics for solar cells,” *Nat. Photonics*, vol. 6, no. 3, pp. 130–132, Feb. 2012.
- [29] K. R. Catchpole and A. Polman, “Design principles for particle plasmon enhanced solar cells,” *Appl. Phys. Lett.*, vol. 93, no. 19, pp. 1–4, 2008.
- [30] H. Kim *et al.*, “Effect of texturing process involving saw-damage etching on crystalline silicon solar cells,” *Appl. Surf. Sci.*, vol. 284, pp. 133–137, 2013.
- [31] A. Velozo, “Crystalline Silicon Photovoltaic Solar Cells using Amorphous Silicon as Dopant Source,” no. October 2012, p. 53, 2012.
- [32] S. H. Altinoluk *et al.*, “Light Trapping by Micro and Nano-hole Texturing of Single-crystalline Silicon Solar Cells,” *Energy Procedia*, vol. 92, pp. 291–296, 2016.

- [33] J. Henrie, S. Kellis, S. Schultz, and A. Hawkins, "Electronic color charts for dielectric films on silicon.," *Opt. Express*, vol. 12, no. 7, pp. 1464–1469, 2004.
- [34] D. Kim, S. Jeong, and J. Moon, "Synthesis of silver nanoparticles using the polyol process and the influence of precursor injection.," *Nanotechnology*, vol. 17, no. 16, pp. 4019–4024, 2006.
- [35] S. Coskun, B. Aksoy, and H. E. Unalan, "Polyol synthesis of silver nanowires: An extensive parametric study," *Cryst. Growth Des.*, vol. 11, no. 11, pp. 4963–4969, 2011.
- [36] C. Giroto and M. Eslamian, "Exploring spray coating as a deposition technique for the fabrication of solution- processed solar cells," no. October 2016, pp. 60–84, 2014.
- [37] Q. T. H. Lamp, R. P. Supply, C. Lens, F. Lens, C. Wheel, and I. Sphere, "Reflectivity and Transmittance measurement setup and procedure," no. 68831, pp. 8–10.
- [38] Labsphere, "Technical Guide: Integrating Sphere Theory and Applications," *Man. Integr. Sph.*, pp. 1–19, 2011.
- [39] HunterLab, "Haze Application Note," vol. 9, no. 6, p. <http://barnett-technical.com/HunterLab%20Haze%20Ap>, 2008.
- [40] Q. T. H. Lamp and R. P. Supply, "External Quantum Efficiency measurement setup and procedure Components," no. 68831.
- [41] "Part II – Photovoltaic Cell I-V Characterization Theory and LabVIEW Analysis Code," 2012. [Online]. Available: <http://www.ni.com/white-paper/7230/en/>. [Accessed: 19-Jan-2017].
- [42] A. Crut, P. Maioli, N. Del Fatti, and F. Vallée, "Optical absorption and scattering spectroscopies of single nano-objects," *Chem. Soc. Rev.*, vol. 43, no. 11, pp. 3921–3956, 2014.
- [43] "Understanding and interpreting box plots." [Online]. Available: <http://www.wellbeingatschool.org.nz/information-sheet/understanding-and-interpreting-box-plots>. [Accessed: 20-Jan-2017].